AGU PUBLICATIONS

JGR

Journal of Geophysical Research: Atmospheres

RESEARCH ARTICLE
10.1002/2016JD026055

Key Points:
- Two subgrid-scale turbulence schemes, 1.5-TKE and CLUBB, were compared in simulations of an Arctic mixed-phase stratocumulus cloud
- Comparing to observations shows that both schemes produce the liquid water profiles within measurement variability but not ice water profiles
- Updraft and downdraft cores are different in size, similar in strength, and composed of both liquid and ice

Supporting Information:
- Supporting Information S1
- Movie S1

Correspondence to:
E. L. Roesler,
eroesler@gmail.com

Citation:
Roesler, E. L., D. J. Posselt, and R. B. Rood (2017), Using large eddy simulations to reveal the size, strength, and phase of updraft and downdraft cores of an Arctic mixed-phase stratocumulus cloud, *J. Geophys. Res. Atmos.*, *122*, 4378–4400, doi:10.1002/2016JD026055.

Received 4 OCT 2016
Accepted 21 MAR 2017
Accepted article online 6 APR 2017
Published online 18 APR 2017

Using large eddy simulations to reveal the size, strength, and phase of updraft and downdraft cores of an Arctic mixed-phase stratocumulus cloud

Erika L. Roesler[1], Derek J. Posselt[2], and Richard B. Rood[3]

[1]Sandia National Laboratories, Albuquerque, New Mexico, USA, [2]Jet Propulsion Laboratory, Pasadena, California, USA, [3]Climate and Space Sciences and Engineering, University of Michigan, Ann Arbor, Michigan, USA

Abstract Three-dimensional large eddy simulations (LES) are used to analyze a springtime Arctic mixed-phase stratocumulus observed on 26 April 2008 during the Indirect and Semi-Direct Aerosol Campaign. Two subgrid-scale turbulence parameterizations are compared. The first scheme is a 1.5-order turbulent kinetic energy (1.5-TKE) parameterization that has been previously applied to boundary layer cloud simulations. The second scheme, Cloud Layers Unified By Binormals (CLUBB), provides higher-order turbulent closure with scale awareness. The simulations, in comparisons with observations, show that both schemes produce the liquid profiles within measurement variability but underpredict ice water mass and overpredict ice number concentration. The simulation using CLUBB underpredicted liquid water path more than the simulation using the 1.5-TKE scheme, so the turbulent length scale and horizontal grid box size were increased to increase liquid water path and reduce dissipative energy. The LES simulations show this stratocumulus cloud to maintain a closed cellular structure, similar to observations. The updraft and downdraft cores self-organize into a larger meso-γ-scale convective pattern with the 1.5-TKE scheme, but the cores remain more isotropic with the CLUBB scheme. Additionally, the cores are often composed of liquid and ice instead of exclusively containing one or the other. These results provide insight into traditionally unresolved and unmeasurable aspects of an Arctic mixed-phase cloud. From analysis, this cloud's updraft and downdraft cores appear smaller than other closed-cell stratocumulus such as midlatitude stratocumulus and Arctic autumnal mixed-phase stratocumulus due to the weaker downdrafts and lower precipitation rates.

Plain Language Summary Low-lying clouds in the Arctic are ubiquitous and important to understand for the near-surface energy balance. These clouds are difficult to measure because of the challenging environment in which they reside. High-resolution models are tools that help fill in knowledge gaps about these clouds. In this work, we compare two different ways to represent fine motion within the cloud and see how the macrophysical properties of the cloud are affected. We found that one representation creates a more energetic cloud, and this type of cloud would exist longer than the other. We also are led to believe in these simulations that these clouds have different internal motions when compared to similar-looking clouds formed at lower latitudes or formed in a different season in the Arctic.

1. Introduction

The areal extent of Arctic sea ice and its rapid decline during the past decade have climatological significance beyond the Arctic [*Stroeve et al.*, 2012]. For example, a connection could exist between the loss of Arctic ice and midlatitude weather patterns [*Francis and Vavrus*, 2012]. Elements of the Arctic environment that can contribute to further sea ice melt include boundary layer stratocumulus clouds. These types of clouds are common in the Arctic and are mostly mixed phase, meaning that they can contain both liquid and ice particles. Because of the ubiquitious nature of these liquid-containing clouds in the Arctic, they have a net positive radiative forcing, warming the surface through most of the year [*Curry et al.*, 1996; *Intrieri et al.*, 2002].

How these mixed-phase clouds persist despite the coexistence of ice and liquid within the cloud is an active scientific question. It is known that these mixed-phase boundary layer clouds contain liquid water at the top of the cloud. Longwave cooling from this liquid layer leads to negative buoyancy, which drives parcels downward into the cloud. There could also be ice precipitation from the cloud. Within the updraft and downdraft cores,

it is believed that ice and liquid water compete to be the dominant phase. Through this paper, we present our findings regarding the properties of the cores in mixed-phase clouds in order to better understand their persistence and longevity.

Several Arctic field campaigns have been conducted during the last decade with goals to obtain statistical properties and insight into the large-scale and internal dynamics involved with mixed-phase clouds' formation, persistence, and decay. For instance, during the SHEBA (Surface Heat Budget of the Arctic) campaign which occurred in the years 1997–1998, surface-based remote sensors were used for year-long measurements [*Shupe et al.*, 2005a]. It was reported that multilayered cloud scenes with all-liquid, all-ice, or mixed-phase clouds were common and that mixed-phase clouds had a higher likelihood of occurring during the transition seasons of spring and autumn. During SHEBA, all-liquid clouds were observed to occur during about 20% of the year, and mixed-phase clouds were observed to occur about 40% of year [*Shupe et al.*, 2005a].

Properties of single-layer mixed-phase stratocumulus clouds were measured during the MPACE (Mixed-Phase Arctic Clouds Experiment) [*McFarquhar et al.*, 2007] field campaign and the Study of Environmental Arctic Change long-term measurements in far northern Canada [*Eicken*, 2013]. It was found that throughout the cloud's height, the liquid-to-ice ratio did not always linearly decrease as cloud temperature decreased. Water in its liquid state could exist at temperatures as low as −31°C [*McFarquhar et al.*, 2007; *de Boer et al.*, 2009]. During the Arctic Summer Cloud Ocean Study conducted in summer 2008, *Shupe et al.* [2013] showed that most of the observed stratocumulus clouds were decoupled from the surface, meaning that surface fluxes were not driving turbulent motion within the cloud.

The ISDAC (Indirect and Semi-Direct Aerosol Campaign) field campaign conducted in April 2008 made measurements of boundary layer clouds during a time of the year when decoupled boundary layer clouds were likely to be observed. Springtime in the Arctic is prior to the onset of extensive and rapid sea ice melt, so surface energy fluxes are usually low from the ocean to the atmosphere. ISDAC was based out of the long-term monitoring DOE ARM (Department of Energy Atmospheric Radiation Measurement) program field site located near Barrow, Alaska, on the North Slope of Alaska. Mixed-phase clouds were previously observed at this location during other campaigns such as SHEBA, MPACE, and First International Satellite Cloud Climatology Project Regional Experiment-Arctic Clouds Experiment [*Barrie*, 1986; *Ghan et al.*, 2007; *Shupe et al.*, 2005b, 2006]. Single-layer mixed-phase stratocumulus clouds were observed on 8 and 26 April.

The focus of this study is the springtime Arctic stratocumulus cloud that occurred on 26 April 2008. In previous numerical studies of this mixed-phase cloud, *Ovchinnikov et al.* [2011] found that the stability and longevity of this mixed-phase cloud was sensitive to the prescribed ice concentration, where too little or too much prescribed ice caused an all-liquid cloud or depleted most of the condensate. It was also found that the stability of the springtime mixed-phase clouds and the turbulent kinetic energy production relies on longwave cooling at the cloud top and the continuous growth of ice particles in the downdrafts. *Ovchinnikov et al.* [2011] and *Morrison et al.* [2012] showed that a precarious relationship exists between the microphysics, turbulence, and other environment components that can either drive the cloud into a stable state, lead to its dissipation, or prevent its formation.

Given the work that has been done investigating the microphysics and the liquid-to-ice ratios of this cloud, we provide further analysis regarding the cores of this mixed-phase cloud with three-dimensional (3-D) large eddy simulations (LES). LES simulations have the ability to resolve vertical motion of the largest eddies of the boundary layer circulation (definition from *Cheng et al.* [2010]) of meso-γ-scale cloud organization. (The meso-γ scale is defined as being 2–20 km in size with a 3–30 min timescales from *Orlanski* [1975].) Two types of turbulent kinetic energy closures are used in this assessment. The first scheme is a 1.5-order turbulent kinetic energy (called 1.5-TKE hereafter) parameterization developed by *Deardorff* [1980]. The 1.5-TKE scheme was developed for simulations that can resolve the turbulent motion of stratocumulus clouds. The second scheme, Cloud Layers Unified By Binormals (CLUBB), is a higher-order closure model that closes the second- and third-order terms of the Reynolds-Averaged Navier Stokes equations via the use of probability distribution functions. A thorough description of CLUBB is given by *Golaz et al.* [2002] and *Larson et al.* [2002]. CLUBB is designed to operate in a consistent manner in many environments and for many types of clouds including boundary layer cloud systems [e.g., *Golaz et al.*, 2002; *Larson et al.*, 2012; *Bogenschutz et al.*, 2013]. However, CLUBB has not been tested at LES scales for an Arctic mixed-phase stratocumulus cloud. We recognize that CLUBB was not intended to be used at these resolutions, but there is a community need to understand the

performance of scale-aware parameterizations in many environments. This paper, therefore, uses CLUBB at LES scales to better understand the updraft and downdraft cores of an Arctic mixed-phase cloud.

This paper aims to answer the following questions:

1. What are the macrophysical differences of the cloud when different subgrid turbulent parameterizations are used?
2. What are the properties (i.e., size, strength, and phase) of the updraft and downdraft cores of this mixed-phase cloud?
3. How do these properties compare with current knowledge of other stratocumulus cloud cores?

To answer these questions, the paper is organized as follows. In section 2, an overview of the turbulent closure schemes is given. Section 3 contains the observational description of the mixed-phase cloud and the model configuration. Section 4 compares the control-run simulations with observations. Section 5 compares the mixed-phase clouds produced by the two turbulence schemes, and section 6 shows how modifications to CLUBB's scheme changes macroscopic properties of the mixed-phase cloud through its computed turbulent kinetic energy. Section 7 presents the sizes, strengths, and phase in the updraft and downdraft cores and compares these findings to current knowledge of other stratocumulus clouds. The summary and conclusions section follows.

2. Model Description

We use SAM (System for Atmospheric Modeling, version 6.8.2) [*Khairoutdinov and Randall*, 2003], a model capable of running in large eddy simulation (LES) or cloud-resolving model configurations, for this study. *Khairoutdinov and Randall* [2003] contains a thorough description of SAM. In SAM, we use the Morrison two-moment microphysics scheme, which predicts the mass and concentration of drops, ice, rain, snow, and graupel [*Morrison et al.*, 2005]. The radiation package is based on the radiation scheme from the National Center for Atmospheric Research Community Atmosphere Model (version 3.0) [*Collins et al.*, 2006]. In SAM, anelastic momentum equations are advanced in time for the resolved wind components, the liquid/ice water static energy, and the total nonprecipitating and precipitating water mixing ratios in Cartesian coordinates. Higher-order moments resulting from the filtered Navier-Stokes equations need closure by a subgrid-scale scheme. Two subgrid-scale turbulence parameterizations, CLUBB version 1.18 and the 1.5-TKE parameterization, are used for closure in SAM.

Deardorff [1980]'s 1.5-TKE turbulence scheme is a three-dimensional turbulence model for stratocumulus-capped mixed layers where the subgrid-scale terms are closed with a gradient-diffusion closures. An example of this closure for buoyancy flux would be $\overline{w'\theta_l'} = -K_h \partial\overline{\theta}_l/\partial z$, where K_h is the subgrid eddy coefficient for scalar quantities given by $(1+2l/\Delta s)\, K_m$, K_m is the subgrid-scale eddy coefficient for momentum given by $0.10\, l\, \overline{E}^{1/2}$, l is the subgrid-scale mixing length, and $\overline{E}^{1/2}$ is the subgrid-scale kinetic energy. The kinetic energy is given by $\overline{E} = \frac{1}{2}(\overline{u'^2}+\overline{v'^2}+\overline{w'^2})$. The subgrid-scale mixing length, l, is set to not exceed the grid scale, $\Delta s = (\Delta x \cdot \Delta y \cdot \Delta z)^{1/3}$, in magnitude. Additional restrictions are placed on the magnitude of the mixing length scale for regions of positive or negative buoyancy [*Deardorff*, 1980].

CLUBB has prognostic equations for the second-order terms and closes third-order terms using probability distribution functions from a preselected family of double Gaussian probability distribution functions. The moments or correlations of the variables are computed by integrating over the probability distribution function. The family of probability distribution functions is chosen to be Gaussian and quasi-normal so that odd-ordered moments do not vanish [*Golaz et al.*, 2002; *Larson et al.*, 2002]. Because the probability distribution function is from the double Gaussian family, the solution is analytic and an equation consisting of the product of the widths, locations, and mean values of the variables is produced. The probability distribution function thus closes the higher-order moments, which are then used to advance the prognostic equations.

This version of CLUBB closes the second-order horizontal winds, $\overline{u'w'}$ and $\overline{v'w'}$, with a gradient-diffusion approach, i.e., $\overline{u'w'} = -K_m \partial\overline{u}/\partial z$ and $\overline{v'w'} = -K_m \partial\overline{v}/\partial z$, where $K_m = c_k L_1 \overline{e}^{1/2}$, c_k =0.548, L_1 is an eddy length scale, and $\overline{e}$ is the subgrid-scale turbulent kinetic energy [*Golaz et al.*, 2002]. The kinetic energy is also given by $\overline{e} = \frac{1}{2}(\overline{u'^2} + \overline{v'^2} + \overline{w'^2})$. Dissipation terms are contained in the second- and third-order prognostic equations. Each of these dissipation terms is also a function of an eddy length scale [*Golaz et al.*, 2002; *Larson et al.*, 2012]. The eddy length scale is calculated from the idea that given a parcel's buoyancy within the vertical column,

Table 1. Vertical Prognostic Quantities in the 1.5-TKE Scheme Based On *Deardorff* [1980] and the CLUBB Scheme From *Golaz et al.* [2002] Where w Is the Vertical Velocity, θ_l Is the Liquid Water Potential Temperature, and q_t Is the Total Water Specific Humidity

Scheme	$\overline{w'\theta_l'}$	$\overline{w'q_t'}$	$\overline{q_t'\theta_l'}$	$\overline{w'^2}$	$\overline{\theta_l'^2}$	$\overline{q_t'^2}$	$\overline{w'^3}$
1.5-TKE	×	×		×			
CLUBB	×	×	×	×	×	×	×

the parcel's vertical displacement is based on its initial kinetic energy. Limits are set on the length scale to maintain numerical stability, and the default maximum value of the length scale in CLUBB is one fourth of the grid size [*Larson et al.*, 2012]. Latent heat release from ice formation is not explicitly taken into account in this version of CLUBB, and ice and precipitation processes are handled in the microphysics parameterizations. More recent development work addresses ice mass in CLUBB. See, for example, *Storer et al.* [2015]. This treatment of ice and precipitation is consistent between the 1.5-TKE and CLUBB schemes. Table 1 lists prognostic variables of the CLUBB and the 1.5-TKE scheme from the filtered Navier-Stokes equations.

3. Description of the Mixed-Phase Cloud and Model Configuration

On 26 April 2008, a single-layered mixed-phase cloud system was observed near Barrow, Alaska. A region of high pressure centered over the Arctic Ocean and weak easterly wind flow was observed at Barrow, Alaska, and pushed a cloud system toward Barrow. The ocean was mostly ice covered at this time [*McFarquhar et al.*, 2011]. Reanalysis products from ERA-40 Interim during 25–26 April 2008 show low-level cloudiness off the coast near Barrow [*European Centre for Medium-Range Weather Forecasts*, 2009]. Figure 1 shows a snapshot of the computed fractional cloud cover from the reanalysis product on 26 April 2008 at 06:00 Greenwich Mean Time (GMT) at ~865 hPa. The cloud, as depicted by the reanalysis, appears on 25 April in the Chukchi Sea between the Russian and Alaskan landmasses. The reanalysis shows the cloud layer to be mostly between 800 and 900 hPa during the 25–26 April 2008 advecting westward, and eventually covering the North Slope. Reports from observations differ slightly. On 26 April 2008, the mixed-phase cloud was actually several hundred kilometers from Barrow over the ocean when in situ aircraft measurements were taken. We thus rely on a combination of information from reanalysis and in situ aircraft measurements to simulate an idealized representation of this Arctic mixed-phase cloud. The aircraft measurements are mainly used to initialize and constrain the microphysics of the LES simulations, and the reanalysis is mainly used for the dynamics initial conditions.

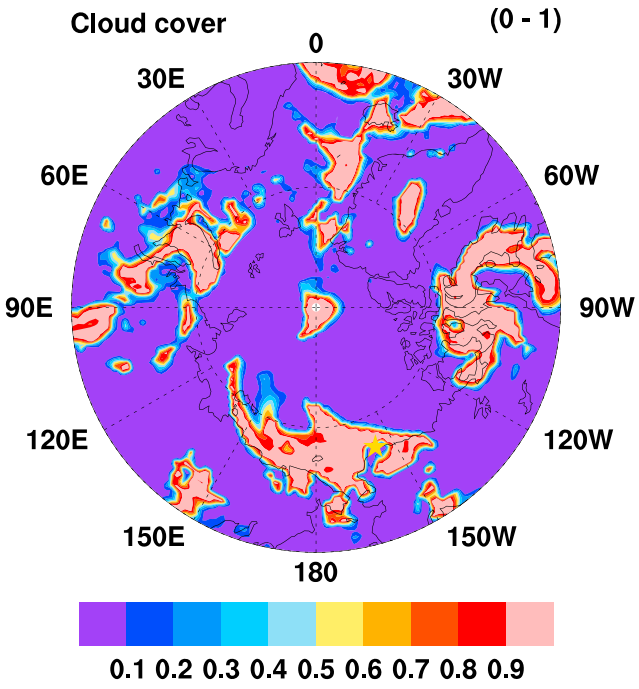

Figure 1. The fractional cloud cover at approximately 865 hPa over the Arctic on 26 April 2008 at 06:00 GMT taken from the ERA-40 Interim reanalysis. The gold star indicates the location of Barrow, Alaska.

The boundary and initial conditions for SAM's surface fluxes, temperature profile, and wind profiles are taken from the DOE ARM site's radar and atmospheric sounding measurements and from the 26 April 2008 aircraft observations. Atmospheric profiles are derived using constrained variational analysis based on European Centre for Medium-Range Weather Forecasts analysis fields [*Zhang and Lin*, 1997; *Zhang et al.*, 2001; *Xie et al.*, 2006]. This technique uses sounding measurements of winds, temperature, and water vapor mixing ratio to interpolate global climate model grid-scale vertical velocity and advective tendencies. The profiles are smoothed to remove noise.

The resultant idealized profiles are shown in Figure 2. The temperature

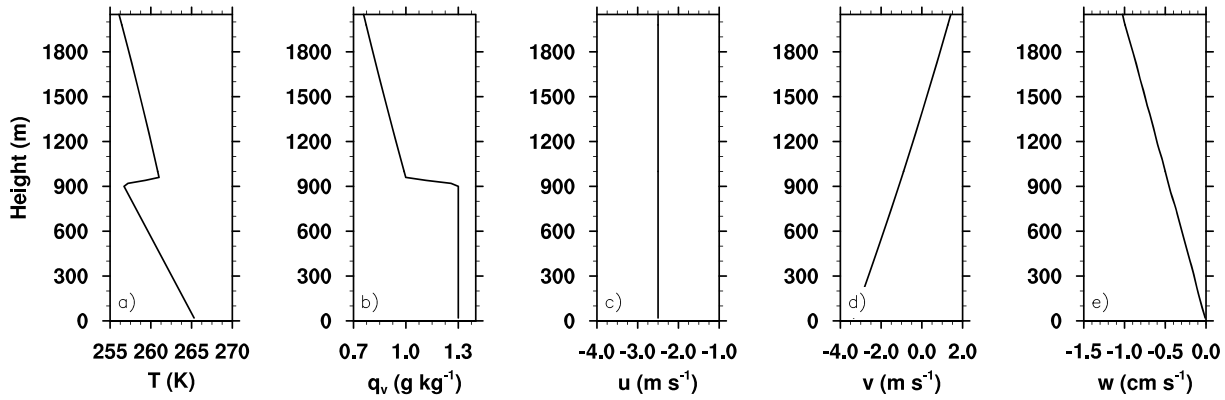

Figure 2. Idealized vertical profiles used for model initialization and large-scale forcing. (a) Temperature (T), (b) water vapor mixing ratio (q_v), (c) zonal wind (u), (d) meridional wind (v), and (e) large-scale vertical wind (w).

and moisture profiles in the lower troposphere were modified to more closely match the structure of the boundary layer at the time and location of the flight. In Figure 2a, the temperature at the surface is 265.3°K and decreases to 256.7°K at 900 m then begins to increase with height to form a temperature inversion. The water vapor is well mixed in the boundary layer from the surface to 900 m (Figure 2b). When the cloud is initially formed in SAM, the increasing temperature and decreasing water vapor with height above 900 m creates a vertically stable atmosphere. Figures 2c–2e show the horizontal and vertical wind profiles of the large-scale flow. The time tendencies of these winds are used to advect the cloud in the LES domain. The simulations are nudged to large-scale winds every 4 h. The temperature and water vapor mixing ratio are not nudged.

The simulation is run for 24 h on a three-dimensional, doubly periodic domain with 120 × 120 × 120 grid points centered at 71.32° north, −156.61° west. A uniform vertical grid is used with grid spacings of $\Delta z = 20$ m starting 20 m above the surface. The horizontal grid spacings are $\Delta x = \Delta y = 100$ m, and the dynamical and radiation time steps are 2 s. The grid spacing and time step were chosen so that numerical stability conditions are satisfied. This configuration defines the control run.

The aerosol size distribution parameters and composition in the cloud microphysical parameterization are prescribed in SAM. The aerosol size distribution mean diameter, D, geometric standard deviation, σ_g, and initial aerosol number concentration, N_A, are initialized as $D = 0.194$ μm, $\sigma_g = 1.48$, and $N_A = 199$ cm^{-3}. These parameters are based on measurements obtained during 26 April 2008 research flights (S. J. Ghan, personal communication, 2010) and compiled by Peter Liu and Mike Earle. Measurements collected during the ISDAC campaign showed the primary aerosol composition to be sulfate mixed with organics, biomass burning, and sea salt [*McFarquhar et al.*, 2011]. *Zelenyuk et al.* [2010] found that most of the larger particles over 0.1 μm in diameter were activated in the cloud and that particle size was the most important parameter for aerosol activation, with sulfate content being of secondary importance. Based on this information, the aerosol composition in SAM is set to be ammonium sulfate, $(NH_4)_2SO_4$, with no insoluble, organic, or sea salt components. A comprehensive study of how aerosol concentration, composition, and size affect cloud droplet number has shown that approximating the aerosol composition as the three-ion ammonium sulfate instead of more complicated molecule is not expected to change the droplet number within the modeled cloud significantly [*Roesler and Penner*, 2010]. A lognormal aerosol size distribution is used to compute the cloud condensation nuclei spectra for the Morrison microphysics, and droplet number concentration is predicted using the aerosol activation parameterization of *Abdul-Razzak and Ghan* [2000].

The ice nucleation is prescribed following the procedure in *Morrison et al.* [2011], *Ovchinnikov et al.* [2011], and *Ovchinnikov et al.* [2014], which eliminates uncertainty in the nucleation mechanism. The ice nucleation is essentially nudged to a prescribed value under specific environmental thresholds of supersaturation and liquid water concentration. The rate is given by

$$\frac{\partial N_i}{\partial t} = \max\left(0, \frac{N_{i0} - N_i}{\Delta t}\right), \quad S_i \geq 0.05 \text{ or } q_l \geq 0.001 \text{ g kg}^{-1}$$
$$\frac{\partial N_i}{\partial t} = 0, \qquad S_i < 0.05 \text{ or } q_l < 0.001 \text{ g kg}^{-1}, \tag{1}$$

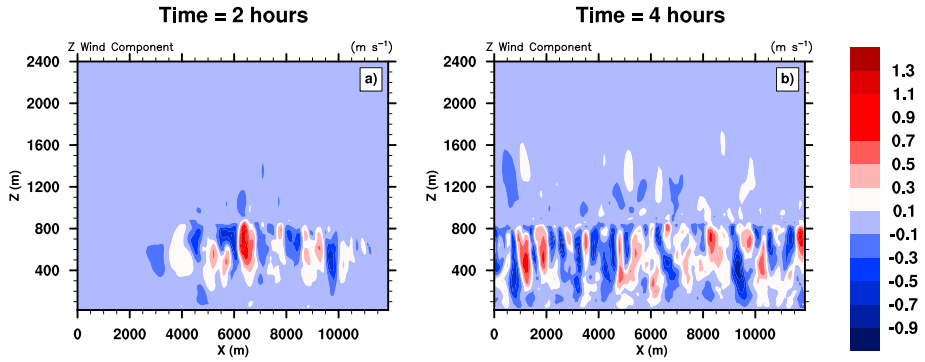

Figure 3. Snapshots of the cross section of the vertical velocity in the 1.5-TKE simulation at (a) 2 h and (b) 4 h. The cross section is taken in the middle of the domain at $y = 6000$ m.

where N_{i0} is the prescribed ice particle concentration, N_i is the model's predicted ice concentration computed after other species' tendencies have been computed in the previous time step, Δt is the model time step, S_i is the fractional supersaturation over ice, and q_l is the liquid water mixing ratio. N_{i0} is set to 0.5 L^{-1}. The sensitivity of the cloud's macrophysical properties to initial ice concentration was tested by doubling N_{i0} to 1.0 L^{-1} and also reducing N_{i0} to 0.1 L^{-1}, similar to the work of *Ovchinnikov et al.* [2011]. The doubling of N_{i0} to 1.0 L^{-1} causes the ice water path to increase at the expense of the liquid water path. The reduction of N_{i0} to 0.1 L^{-1} causes the ice water content to be significantly smaller than what was observed. The cloud's response to changes in prescribed ice concentration is consistent with *Ovchinnikov et al.* [2011], who also tested ranges of N_{i0}. To maintain macrophysical features of a mixed-phased stratocumulus cloud with nonzero liquid and ice water paths, we determine that $N_{i0} = 0.5$ L^{-1} to be the best value for prescribed ice concentration. Comparison of N_{i0} to in-cloud observations occurs in section 4.

The control run simulation of the Arctic mixed-phase cloud starts at GMT 117.5 and runs for 24 h until 118.5 GMT. The first 4 h are considered spin-up time in which the turbulence, liquid water path, and ice water path are developed in the LES domain. An example of this spin-up time is shown in Figure 3, where a cross section of the three-dimensional vertical velocity is shown at $y = 6000$ m at 2 and 4 h into the simulation with the 1.5 TKE scheme. At 2 h into the simulation, the updraft and downdraft cores have not developed throughout the domain. At 4 h, the updraft and downdraft cores extend throughout the domain and both liquid and ice are present (shown later).

4. Control-Run Simulations Compared With Observations

We next compare properties of the cloud from the simulations with the observations. We emphasize at the outset that the goal is not to replicate the observed cloud. Instead, we aim to simulate a persistent liquid-topped mixed-phase cloud and highlight differences between the real cloud and the simulations upon which it is based. This also documents the simulated clouds' sensitivity to changes in the turbulence representation.

Profiles of the cloud's domain-averaged liquid number concentrations, ice number concentrations, liquid water mass mixing ratio, and ice water mass mixing ratio are compared with ISDAC aircraft measurements in Figure 4. Measurements of the cloud microphysical and macrophysical properties were obtained from a 100 km aircraft flight leg within the cloud. The flight number was 31 (see http://www.acrf-campaign.arm.gov/idsac/flighttable.pdf), and the total aircraft flight time was about 4 h in duration. The measurements used here are when the aircraft porpoised and flew in constant-altitude legs between 250 m and 1000 m above the surface. These data were then binned by altitude into 20 m increments. The aircraft measurements showed most of the liquid to be contained between 600 and 900 m. Ice was measured in the cloud from 380 m to 900 m, and it is estimated that small particles (low mass and high number) were between 700 m and 800 m and larger particles (high mass and low number) were between 400 m and 700 m.

Both the CLUBB and 1.5-TKE schemes reproduce a maximum in liquid water mass mixing ratio near 800 m. The 1.5-TKE scheme overpredicts the liquid mass, while the CLUBB scheme underpredicts the liquid mass compared to the observations. The liquid number concentration maxima is better represented by both

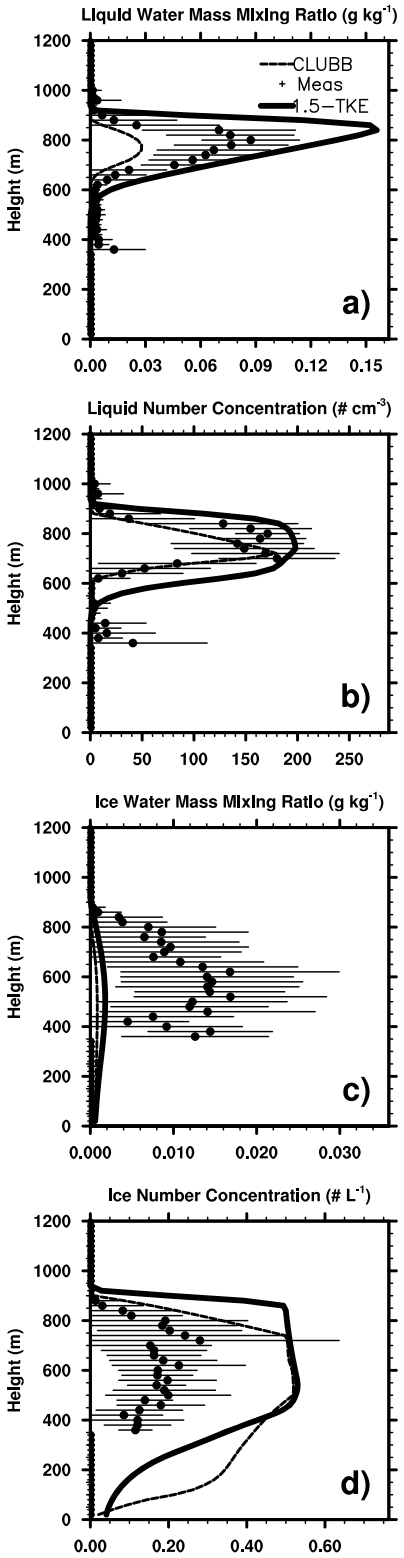

Figure 4. Comparison of the profiles of the average of the aircraft measurements (dots) with the average of the simulations using the 1.5-TKE scheme (solid line) and CLUBB (dashed line) for the (a) liquid water mass mixing ratio, (b) liquid number concentration, (c) ice water mass mixing ratio, and (d) ice number concentration. The aircraft measurements were binned into the model's vertical grid levels and plotted here at each midpoint of the model's vertical grid levels. The horizontal lines on the dots are the standard deviation of the mean of the measurements.

schemes than the mass mixing ratio. An increase in liquid number and mass concentration was measured by the aircraft at 380 m, and neither scheme reproduces this feature. The model's ice number concentration is at least twice as much as was measured, and both schemes have less ice water mass mixing ratio by nearly an order of magnitude.

Constraining ice crystal concentration has been a method of bringing the numerical cloud microphysics closer to the measured values. It could be inferred from Figure 4d that choosing $N_{i0} = 0.1\ L^{-1}$ would bring the ice number concentration in the simulations closer to the measurements. However, recall (from section 3) that this causes the liquid water to increase and the ice water to decrease causing the cloud to be mostly all liquid. The modeled cloud has the most macrophysical similarity to the measured cloud with the value of $N_{i0} = 0.5\ L^{-1}$. We tested the variance and mean radius of the modified gamma distribution to exclude the high concentration, low mass cloud particles. This was found to have little effect on the ice number concentration and ice mass mixing ratio, suggesting that additional work is needed to fit this microphysics scheme to this mixed-phased cloud's liquid and ice concentrations.

Differences between measured and simulated ice water and liquid water are not uncommon in high- and low-resolution simulations of mixed-phase clouds. *Avramov and Harrington* [2010] and *Avramov et al.* [2011] had similar results of underpredicting ice water path using a two-moment microphysics scheme and a bin microphysics scheme with a Smagorinsky-type closure scheme for turbulence, respectively. *Solomon et al.* [2011] used a nested simulation of the Weather Research and Forecasting model using bulk microphysics and a nonlocal-K closure scheme and also underpredicted ice water path. Conversely, in a model intercomparison with single-column models and cloud-resolving models of mixed-phase clouds in the fall, the ice water path was better matched to observations than the liquid water path [*Klein et al.*, 2009]. Other simulations have brought closer agreements between measurements and models for all phases of water in mixed-phase clouds through the use of spectral bin microphysics as shown by *Fan et al.* [2009] or adaptive habit models [e.g., *Sulia et al.*, 2014].

We recognize the reported measurement bias of ice particle mass and concentration in aircraft measurements. *Field et al.* [2006] note that ice water content can be overestimated by 20%–30% by probes (which is not enough to account for the differences between the simulations and measurements presented here). The probes measure ice particles larger than 100 μm, and although shattering can cause ice concentrations to be positively biased, methods were undertaken to compensate for any bias during data postprocessing. It should be noted that the ice crystals with diameters smaller than 100 μm are not expected to contribute significantly to the ice mass mixing ratio, so shattering cannot account for observations being an order of magnitude greater than the simulations in this study. Given this information, the measured ice concentration should be lower than what is shown in Figure 4d, which makes the model bias even higher.

Despite the differences in the magnitudes between the observed and simulated ice concentrations and masses, both schemes produce a mixed-phase cloud with characteristics observed during ISDAC: a liquid layer near cloud top and ice precipitation below. We assume that these are suffcient conditions to continue analysis regarding core properties of mixed-phase clouds. We proceed with comparing the macrophysical properties of the cloud produced with the subgrid-scale turbulence schemes in the next section.

5. Control-Run Results With CLUBB and the 1.5-TKE Schemes

The evolutions of the mixed-phase stratocumulus cloud during the 24 h simulation period for both the 1.5-TKE and CLUBB schemes are shown in Figure 5. As noted above, CLUBB's predicted liquid water mass mixing ratio is smaller than the liquid water mass mixing ratio predicted by the 1.5-TKE scheme. Further differences between the schemes can be seen in the first few hours of the simulation as the model is spinning up. While the 1.5-TKE scheme has little-to-no liquid water in the first 4 h (Figures 5a and 5c), the CLUBB scheme has both a liquid and ice profile. However, as time progresses, the CLUBB cloud liquid layer thins (Figure 5b), the cloud top decreases by 200 m, and eventually (if the simulation is allowed to run longer than 24 h), the cloud will dissipate to the point where the boundary layer will not be capped by any liquid water or ice. Conversely, the 1.5-TKE scheme shows positive cloud-top growth with increases in the liquid and ice water mass mixing ratios (Figures 5a and 5e). The liquid layer depth increases in time (Figure 5a).

The mixed-phase cloud evolves into differing states (i.e., opaque cloud versus thin cloud) depending on the scheme. The cloud with the 1.5-TKE scheme contains more liquid and is more opaque than the cloud with

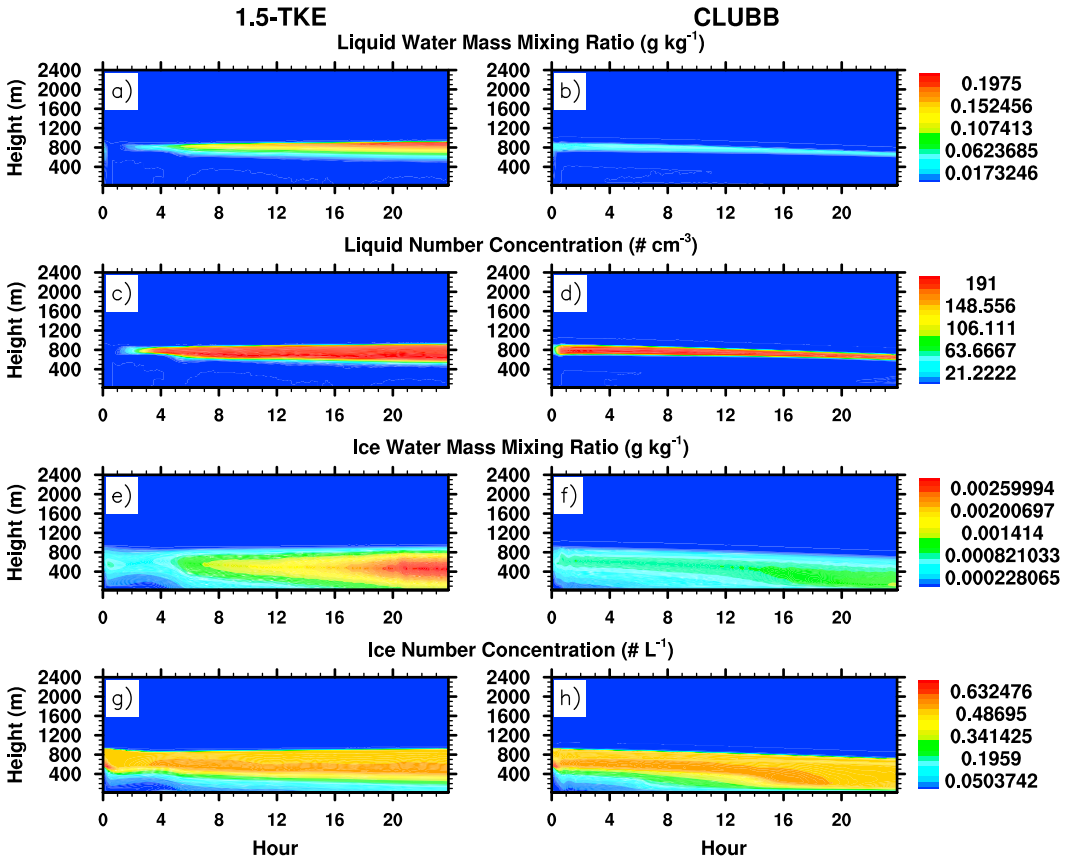

Figure 5. Evolution of the domain-averaged cloud profiles by height of (a and b) liquid water mass mixing ratio, (c and d) liquid number concentration, (e and f) ice water mass mixing ratio, and (g and h) ice number concentration for the 1.5-TKE scheme (Figures 5a, 5c, 5e, and 5g) and the CLUBB (Figures 5b, 5d, 5f, and 5h) during the 24 h simulation period.

CLUBB. This evolution has an effect on the downwelling longwave surface flux. *Turner et al.* [2007] showed the longwave fluxes become insensitive to increases in liquid water path for liquid water paths greater than about 40 g m^{-2}. Figure 6 shows the liquid water path of the mixed-phase cloud as a function of the computed downwelling longwave surface flux. As the liquid water content with the 1.5-TKE simulation becomes established for liquid water paths $\geq$30 g m^{-2}, the downwelling longwave radiation flux at the surface becomes constant at 260 W m^{-2}. However, the predicted liquid water path when CLUBB is used is less than 15 g m^{-2} throughout the cloud's lifetime, peaking at the beginning of the simulation.

The loss of liquid in the cloud produced by CLUBB without an increase in ice mass causes the atmosphere to become more humid. Figure 7 shows this behavior in the profiles of the water vapor mixing ratio, q_v, and the temperature, T, at 4, 10, 16, and 22 h into the simulation. The q_v profiles produced by CLUBB show a steep increase of water vapor between the surface and 150 m which increases in time. We surmise that the anomalously low value of $q_v \approx 0$ at the surface in the CLUBB simulation is a physical inconsistency that is intentionally in the CLUBB scheme, and development efforts will be made to correct it. Recall that surface-based turbulent fluxes of heat and moisture were prescribed to be near zero in these simulations; thus, little-to-no energy perturbations are available to lift the 1.5 g kg^{-1} of water vapor at 150 m vertically to colder temperatures. Above 900 m, the cloud produced with CLUBB shows a larger water vapor mixing ratio than the 1.5-TKE cloud, but low turbulent kinetic energies and eddies (described further in Figure 8) will not entrain water vapor into the cloud top. Thus, the water vapor is essentially not available to the cloud for condensation and particle growth. In the simulation using the 1.5-TKE scheme, the surface value of q_v remains similar to the imposed initial condition value of 1.3 g kg^{-1}. The water vapor mixing ratio remains nearly constant throughout the 24 h simulation in the layer between 200 m and 600 m, which is below the liquid layer. From 600 m to 800 m, q_v is depleted and is converted to liquid water. Above 850 m, the water vapor concentration steadily decreases.

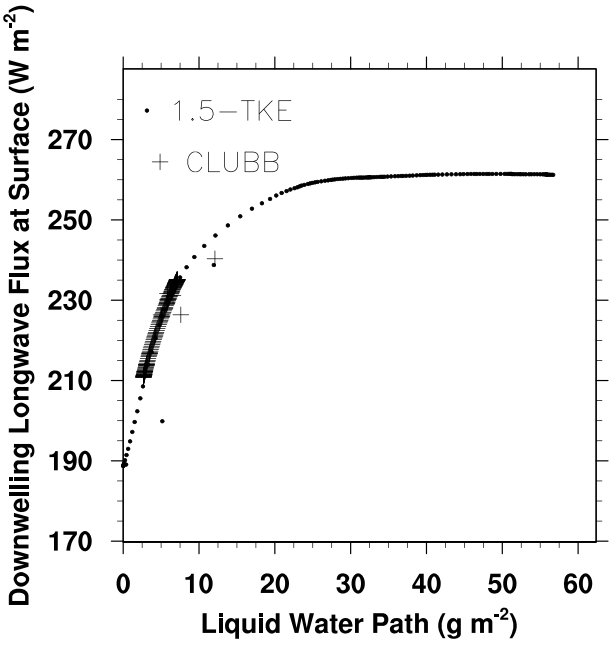

Figure 6. Downwelling longwave radiation flux at the surface as a function of liquid water path for the 1.5-TKE (dots) and CLUBB (plus marks) mixed-phase clouds. Each data point represents the domain-averaged value every 600 s in time.

Moisture sources for the maintenance and stability of the mixed-phase cloud have been explored by *Ovchinnikov et al.* [2011] and by *Solomon et al.* [2011]. *Ovchinnikov et al.* [2011] show that turbulent eddies from the cloud layer need to access the moisture at the surface if the cloud is to persist. *Solomon et al.* [2011] found that the mixed-phase cloud is maintained by a downgradient transport of water vapor by turbulent fluxes from a specific humidity inversion above the cloud top. *Qiu et al.* [2015] have confirmed an above-cloud moisture source via 3 years of observations at the NSA site. CLUBB is not accessing moisture source either above the cloud or below cloud base.

Stratocumulus clouds that are decoupled from the surface need a large-enough liquid water path to drive in-cloud turbulence, which relates to the strength of the cloud-top temperature inversion. The lack of liquid in the CLUBB simulation (Figure 5b) affects the temperature inversion at cloud top (Figure 7). The 1.5-TKE temperature inversion is 77% smaller than the CLUBB inversion at 4 h into the simulation (0.0318 K m^{-1} for 1.5-TKE compared to 0.0414 K m^{-1} for CLUBB) due to CLUBB's more established liquid layer in the spin-up period. However, with CLUBB, at 22 h into the simulation the cloud-top inversion decreases nearly in half to 0.0235 K m^{-1}. Contrast this with 1.5-TKE scheme where the strength of the temperature inversion increases to 0.0812 K m^{-1}. With CLUBB, the less established liquid layer results in reduced radiative cooling, which subsequently impacts the temperature inversion, the cloud-top moisture jump, and the in-cloud dynamics. By the end of the simulation, the liquid water path decreased from 6.5 g m^{-2} to 2 g m^{-2} compared to the 1.5-TKE scheme which increased from 4 g m^{-2} to 54 g m^{-2}. Figure 7 shows that in the CLUBB simulation, the moisture jump and the height of the temperature inversion decreases in time. This suggests that more water vapor is

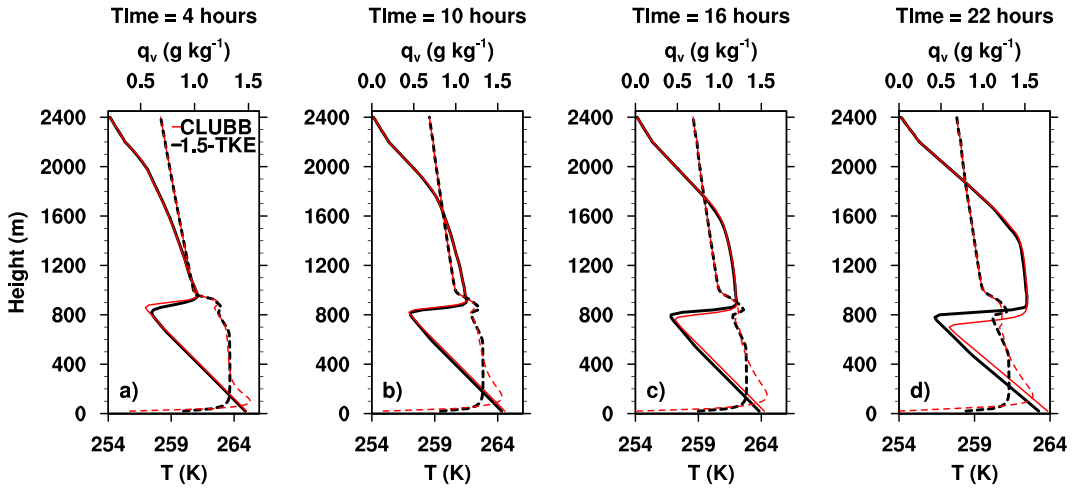

Figure 7. Profiles of the domain-averaged water vapor mixing ratio, q_v (dashed), and temperature, T (solid), from the 1.5-TKE (in black) and CLUBB (in red) schemes. The profiles are at (a) 4, (b) 10, (c) 16, and (d) 22 h into the simulation.

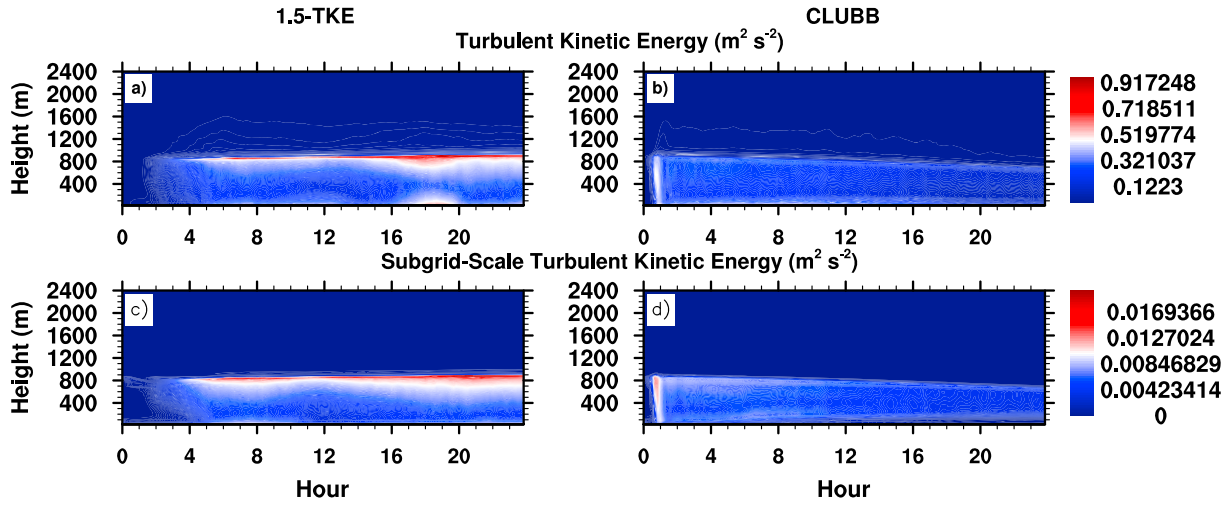

Figure 8. The domain-averaged time evolution by height of the resolved (a and b) and subgrid-scale (c and d) turbulent kinetic energy profiles in time for the 1.5-TKE (Figures 8a and 8c) and CLUBB (Figures 8b and 8d) schemes.

entrained to the area directly above the cloud top, creating a humid layer above the temperature inversion. This is different from the 1.5-TKE situation, where the moisture jump and temperature inversion strengthen in time.

The macrophysical differences just explained in the clouds' liquid water paths and opacities produced by the two schemes is related to the amount of dissipative energy each subgrid scheme calculates, which directly affects the energy of the boundary layer profile. We explain a potential path to reducing the macrophysical differences in the clouds produced by the two schemes in the next section. We will show that CLUBB's turbulence is more dissipative than 1.5-TKE turbulence and how to decrease the dissipation.

6. Reducing CLUBB's Dissipative Energy

The domain-averaged and time evolution of the resolved and subgrid-scale turbulent kinetic energies for the 1.5-TKE and CLUBB schemes are shown in Figure 8. CLUBB's resolved and subgrid-scale turbulent kinetic energy is much smaller throughout the entire simulation than the 1.5-TKE's kinetic energy with the exception of the first hour in the spin-up period. At the surface, the CLUBB simulation's subgrid-scale turbulent kinetic energy is, at times, an order of magnitude smaller than the 1.5-TKE simulation. At the end of the simulation, the domain-averaged value for the resolved turbulent kinetic energy in the 1.5-TKE simulation is 0.15 $m^2\ s^{-2}$, whereas the CLUBB simulation is 0.03 $m^2\ s^{-2}$.

To see how subgrid-scale turbulent kinetic energy impacts the liquid water content, we performed a sensitivity test by turning off the subgrid-scale turbulence parameterizations and found that both the total kinetic energy and liquid water content decreased. Thus for the CLUBB scheme (Figures 8b and 8d), more kinetic energy is needed to maintain the liquid water path. Reducing CLUBB's dissipative energy should increase the liquid water path of the cloud, which can be achieved by two methods. The first is by increasing the length scale (section 6.1), and the second is by increasing the horizontal grid size (section 6.2).

6.1. Increasing the Length Scale

The energy dissipated in the subgrid scale needs to be reduced to increase the liquid water path. In CLUBB, energy dissipation, ϵ, is a function of the grid spacing [e.g., *Golaz et al.*, 2002]. For example, energy dissipation for the vertical velocity variance, $\overline{w'^2}$, is computed from

$$\epsilon = \frac{C}{\tau}\overline{w'^2} - \nu\nabla^2\overline{w'^2}, \tag{2}$$

where the first term is a Newtonian damping term inversely proportional to a characteristic dissipation timescale, τ, and the second term is a background diffusion term used to damp small-scale noise and set to be much smaller than all other terms. In equation (2), C and ν are constants set to control damping.

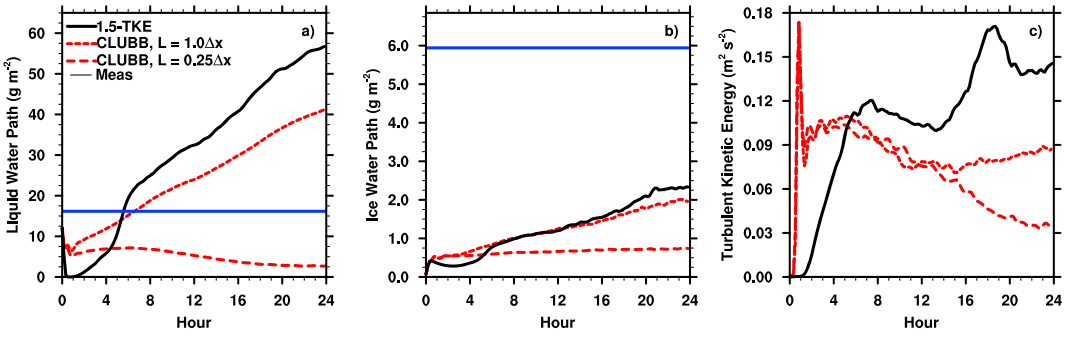

Figure 9. Domain-averaged (a) liquid water path, (b) ice water path, and (c) resolved turbulent kinetic energy in time for the mixed-phase clouds produced by using the 1.5-TKE scheme (black solid line), CLUBB with the default length scale limitation (red large dashed line), and CLUBB with a fourfold increase in the length scale limitation (red small dashed line). The average of the aircraft measurements for liquid and ice water paths is shown as a solid blue line in Figures 9a and 9b in time for comparison.

The characteristic dissipation timescale, τ, is a ratio of the eddy length scale, L, and a characteristic velocity scale, given in equation (2),

$$\tau = \frac{L}{\sqrt{\bar{e}}}.$$

The length scale, L, is limited in CLUBB by the horizontal grid spacing, Δx and Δy, by $L = \alpha \min(\Delta x, \Delta y)$, where by default $\alpha = 0.25$ [*Larson et al.*, 2012]. To decrease dissipation in CLUBB, the length scale was increased to $L = 1.0 \min(\Delta x, \Delta y)$. This causes a larger value of τ, then a smaller Newtonian damping in equation (6.1), and smaller energy dissipation, ϵ.

Increasing the limit on the length scale causes a twentyfold increase in liquid water path, a threefold increase in ice water path, and a threefold increase in resolved turbulent kinetic energy (Figure 9), which brings the macrophysical properties of the CLUBB simulation closer to the 1.5-TKE's and aircraft-measured properties. *Larson et al.* [2012] explain that in CLUBB, L represents the size of the large eddies. By choosing L to be a fraction of the grid box size, the host model will better resolve the eddy motion. We can then infer that for the resolution chosen in this study ($\Delta x = \Delta y = 100$ m, $\Delta z = 20$ m), some eddies were not resolved. The subgrid-scale scheme needed to be more active at this resolution, and diagnosing a larger L improved the solution. We surmise, but have not tested, that a length scale between 0.25 and 1.0 might cause the liquid content to better match the observed value.

6.2. Increasing Horizontal Grid Size

The horizontal grid size can also be increased to reduce the dissipative energy in CLUBB. We simulated the mixed-phase cloud using both the 1.5-TKE and CLUBB schemes over a range of increasing horizontal grid spacings from 50 m to 2500 m (Table 2). In all experiments, the model configuration and setup is identical to what was described in section 3 with the exception of the horizontal grid size. The liquid and ice water paths at the end of the simulation for both schemes are reported in Table 2. As expected, increasing the resolution when CLUBB is used causes the liquid water path to increase in the simulations when $\Delta x = 1000$ m and

Table 2. Horizontal Grid Box Sizes and Domain Sizes of Resolution Sensitivity Tests With the Liquid Water Path and Ice Water Path at the End of the Simulation for Each Resolution Test

Horizontal Grid Box Size $\Delta x \times \Delta y \times \Delta z$	Domain Size on an Edge (km)	Liquid Water Path (g m^{-2}) at 24 h		Ice Water Path (g m^{-2}) at 24 h	
		1.5-TKE	CLUBB	1.5-TKE	CLUBB
50 m × 50 m × 20 m	6	72.5	9.60	0.08	0.12
100 m × 100 m × 20 m	12	56.7	2.67	2.33	0.74
1000 m × 1000 m × 20 m	120	62.4	47.8	2.55	1.65
2500 m × 2500 m × 20 m	300	0.59	47.7	0.006	1.18

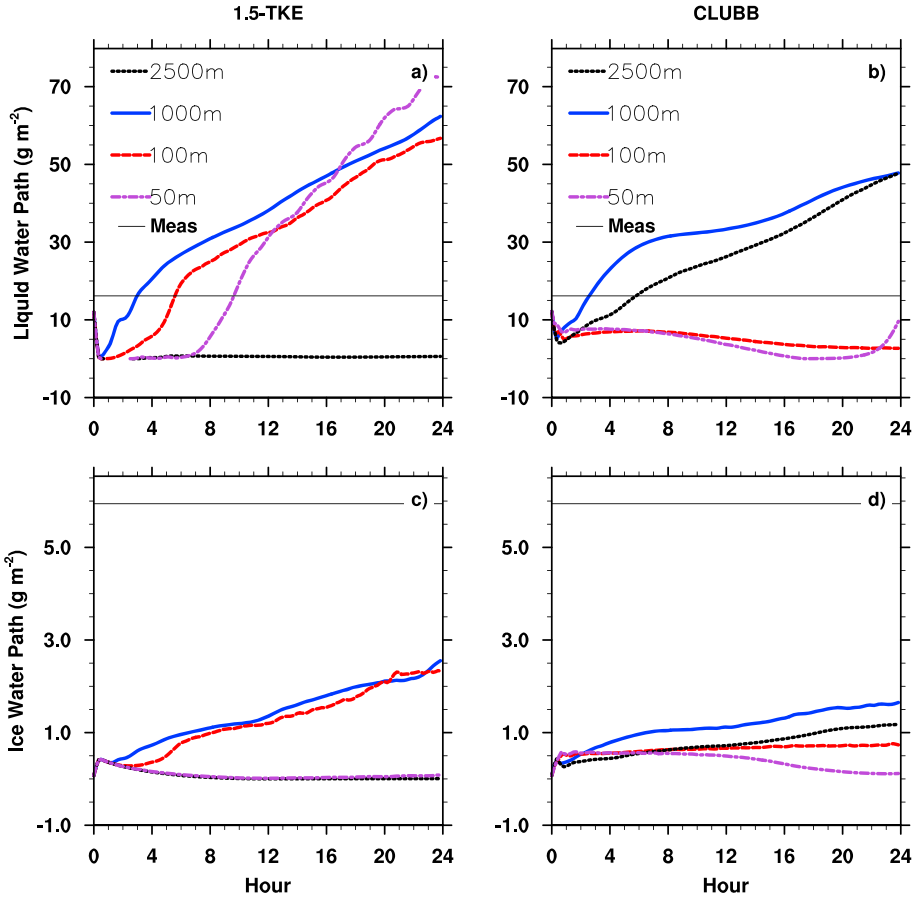

Figure 10. Domain-averaged (a and b) liquid water path and (c and d) ice water path in time with various horizontal grid box sizes for the 1.5-TKE (Figures 10a and 10c) and CLUBB (Figures 10b and 10d) schemes. The average liquid water path and ice water path from the aircraft measurements is shown as a solid line (Meas) for comparison in each of the plots.

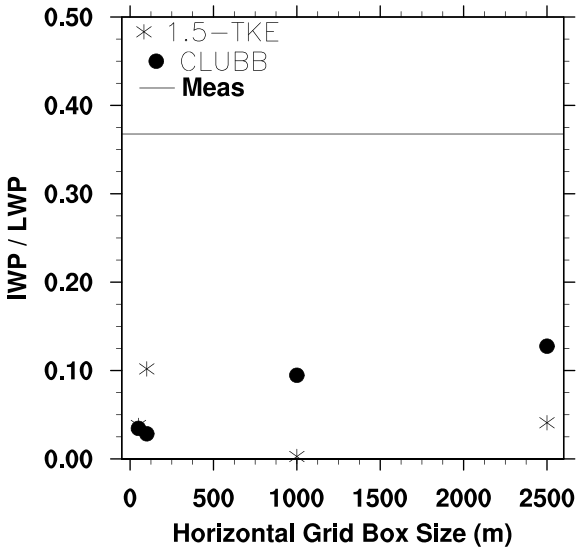

Figure 11. Changes to the ratio of ice water path to liquid water path as horizontal grid box size is increased when the 1.5-TKE (asterisk) and CLUBB (dots) schemes are used. The aircraft value is shown for comparison as a solid line (Meas).

2500 m (Figure 10). However, the cloud at these resolutions has too much turbulent kinetic energy, and the liquid water path continues to increase, eventually exceeding the average aircraft value (16.2 g m^{-2}). The ice water path shows little-to-no sensitivity to resolution in the CLUBB scheme. We suspect that this is due to the constraints on the ice number concentration (via equation (1)). The temperature inversion at $\Delta x = 2500$ m resolution with CLUBB is also stronger than at the control run resolution of 100 m (not shown). *Cheng et al.* [2010] have shown in simulations of warm stratocumulus clouds that liquid water path increases with resolution due to the energy (resolved and subgrid-scale) shifting to larger scale with increased circulation.

The 1.5-TKE scheme produces a mixed-phase cloud at $\Delta x = 100$ and 1000 m grid resolutions and a mostly liquid cloud at 50 m resolution. At 2500 m resolution, the 1.5-TKE scheme has difficulty maintaining a steady state mixed-phase cloud with any ice water path. The overall sensitivity to resolution of mixed-phase clouds is best shown as the ratio of ice water path and liquid water path with increasing horizontal grid box size (Figure 11). Both schemes produce ratios that are at least a factor of 3 smaller than the aircraft measured values for all resolutions. CLUBB appears to converge with increasing Δx, implying a scale awareness for $\Delta x \geq 1000$ m, whereas the 1.5-TKE scheme does not. Potential follow-on work would be understanding resolution convergence for each scheme while maintaining the macroscopic liquid and ice water paths of this mixed-phase cloud.

7. Properties of the Updraft and Downdraft Cores

Now that the macroscopic properties (i.e., liquid and ice water paths, temperature, and energy) of the mixed-phase cloud simulated by the two subgrid-scale turbulence schemes has been presented in the previous sections, we will show how these macroscopic properties impact the core sizes, strength, and phase of the mixed-phase cloud. This will answer our second and third questions asked in section 1.

First, the locations of the updraft and downdraft cores are identified with an algorithm that marches through every point at every level at every time step. For a point to be classified as an updraft, two conditions are required: (1) the virtual potential temperature at an (x, y) point has to be greater than the mean virtual potential temperature at that height and (2) the sum of the vertical velocity at that point and at the point height directly above it have to be greater than zero. For an area to be classified as a downdraft, the opposite conditions are required. That is, (1) the virtual potential temperature at that (x, y) point has to be less than the mean virtual potential temperature at that height, and (2) the sum of the vertical velocity at that point and at the point directly above it has to be less than zero. If neither the updraft nor downdraft criteria is meant, then the point is classified as having neutral vertical motion.

Cross-sectional snapshots of the locations identified as vertical velocity updrafts and downdrafts are shown in Figures 12 and 13 for the cloud simulated with the 1.5 TKE and CLUBB schemes, respectively. When the 1.5 TKE scheme is used, the updrafts and downdrafts appear to organize themselves into larger areas of generally positive or generally negative vertical motion by 4 h into the simulation for below-cloud base and throughout the domain at later times in the simulation. (See, for example, Figures 12k, 12l, 12o, and 12p.) This is meso-γ-scale organization of large areas of positive or negative vertical motion, and it has been observed in other Arctic mixed-phase clouds [*Shupe et al.*, 2008]. Within the larger positive and negative vertical motion areas are highly asymmetric and complex smaller cores. However, the mixed-phase cloud produced with CLUBB is different: the updrafts and downdrafts remain interspersed without larger organization and get weaker in time as the cloud dissipates. This is consistent and to be expected given the lower turbulent kinetic energy and higher dissipation in the control-run CLUBB simulation. For reference, the domain-averaged updrafts and downdrafts are shown for the 1.5-TKE and CLUBB simulations in Figure 14, again confirming the lower energy CLUBB simulation produces weaker updrafts and downdrafts than the 1.5-TKE simulation.

Both simulations appear to produce the Rayleigh-Bérnard convective cellular structures as observed and documented in marine stratocumulus [*Feingold et al.*, 2010]. This means that when the Rayleigh number exceeds its critical value ($Ra > Ra_c$), convection develops. The Rayleigh number is given by $Ra = \alpha g \Delta T h^3/(\nu\chi)$, where α is the thermal expansion coefficient, g is the gravitational acceleration, h is the separation between two horizontal surfaces with a temperature gradient, ν is the kinematic viscosity, and χ is the thermal diffusivity. For atmospheric convection in stratiform clouds, ν and χ are replaced by eddy viscosity and eddy diffusivity [*Krishnamurti*, 1975; *Feingold et al.*, 2010]. Assuming that our domain is large enough to contain a sample of organized convective cellular structures, this mixed-phase cloud has approximately a 10°C temperature gradient and a horizontal surface separation of approximately 1 km, giving $Ra \approx 10^6$, which exceeds $Ra_c \approx 10^3$. Thus, convective cellular structures are supported in this cloud.

A closed-cellular convective structure is the preferred configuration for this cloud where few, if no, cloud gaps are seen in the domain. The closed-cellular convective structure is best seen in the three-dimensional snapshot of vertical velocity and precipitation in Figure 15 and the supporting information Movie S1. The movie shows that the 1.5-TKE simulation produces near-constant cloud cover where very few gaps in the cloud are seen in the domain. In midlatitude clouds, closed-cellular structures are driven by cooling at the cloud top with large areas of moderate updrafts and small areas with strong downdrafts [*Helfand and Kalnay*, 1983].

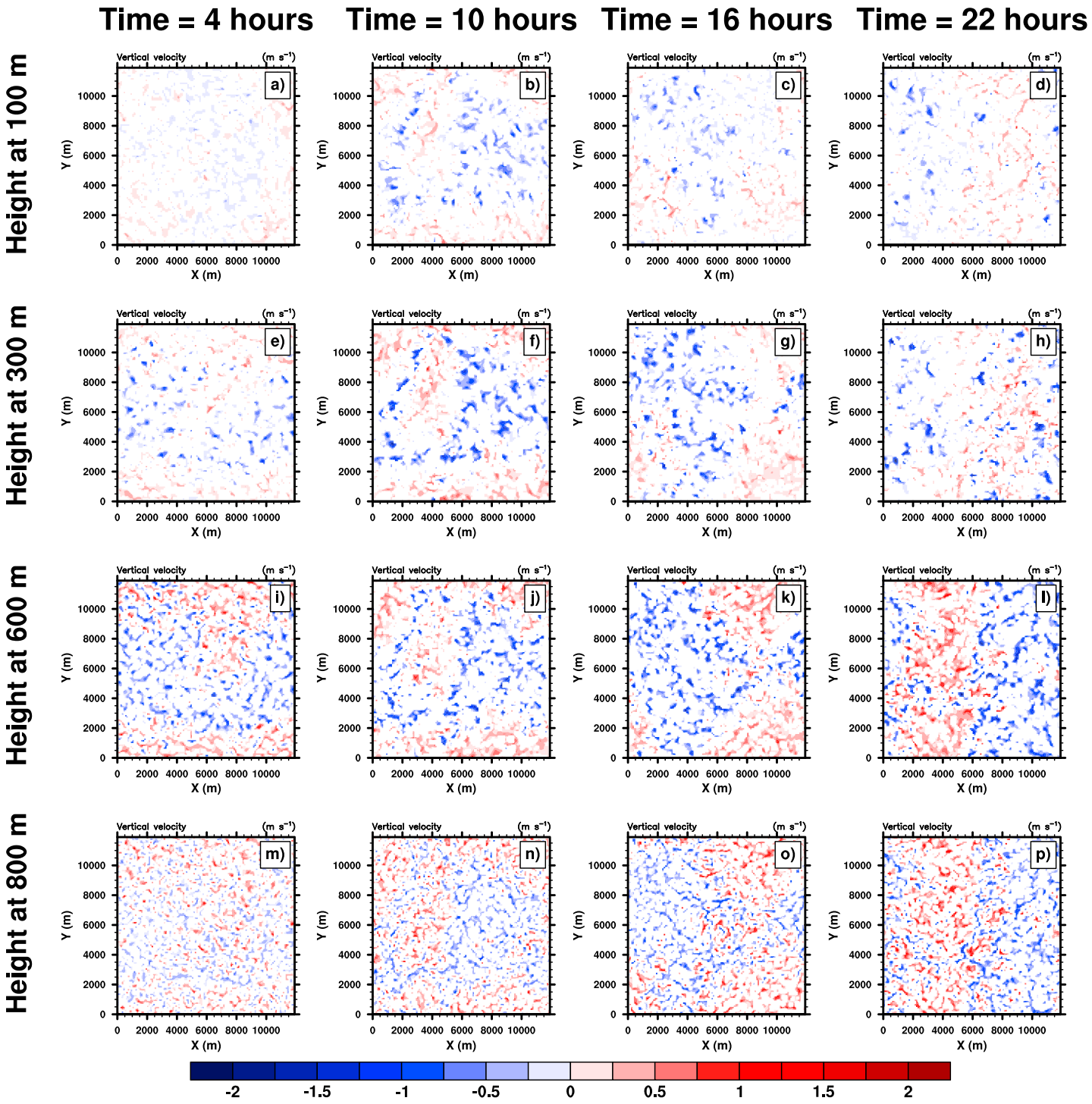

Figure 12. Snapshots of the vertical velocity (m s^{-1}) in the updraft (red) and downdraft (blue) cores taken at (a, e, i, and m) 4, (b, f, j, and n) 10, (c, g, k, and o) 16, and (d, h, l, and p) 22 h into the simulation at 100 (Figures 12a–12d), (Figures 12e–12h) 300, (Figures 12i–12l) 600, and (Figures 12m–12p) 800 m above the surface while using the 1.5-TKE scheme.

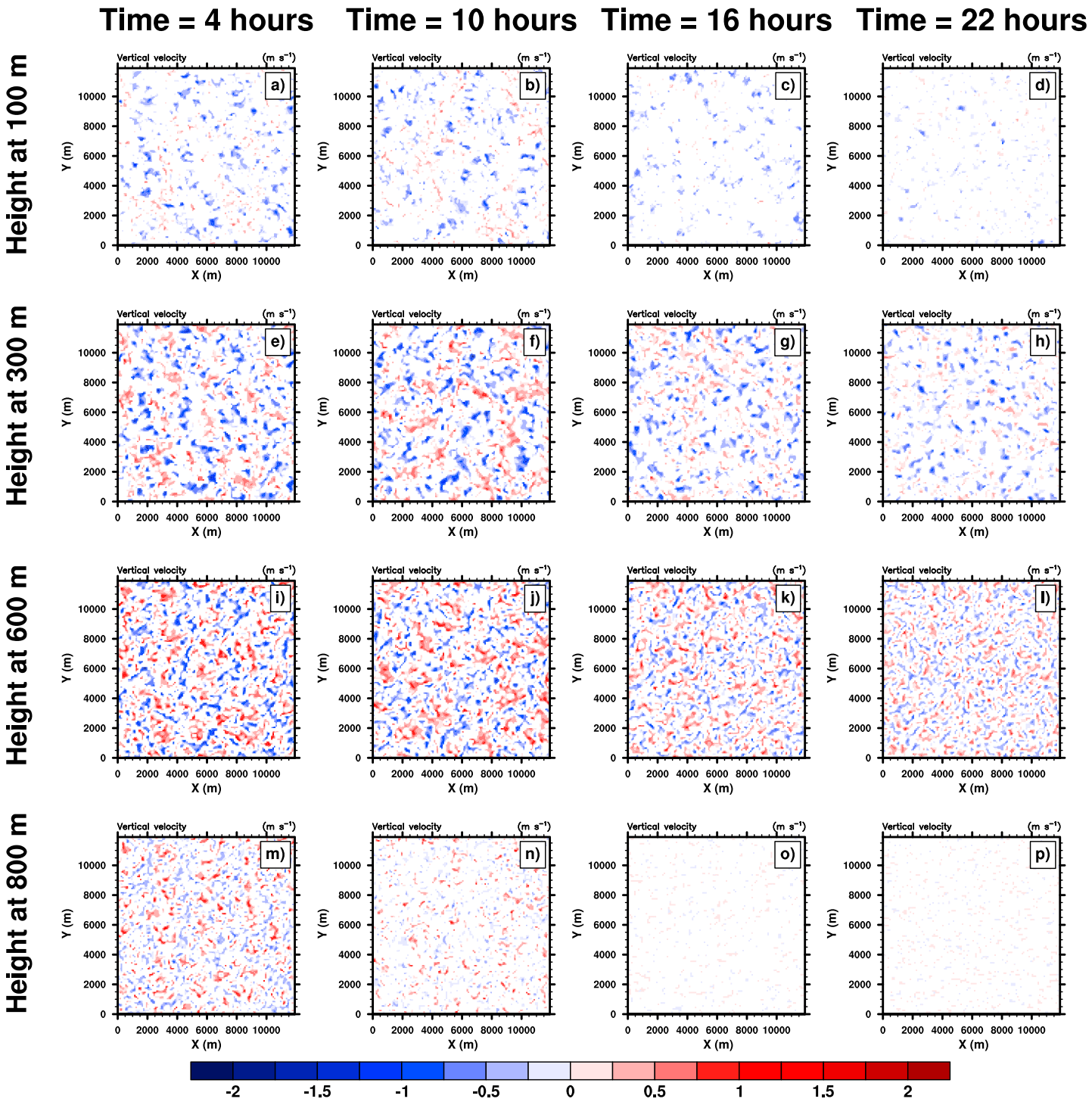

Figure 13. Snapshots of the vertical velocity (m s^{-1}) in the updraft (red) and downdraft (blue) cores taken at (a, e, i, and m) 4, (b, f, j, and n) 10, (c, g, k, and o) 16, and (d, h, l, and p) 22 h into the simulation at 100 (Figures 13a–13d), 300 (Figures 13e–13h), 600 (Figures 13i–13l), and 800 m (Figures 13m–13p) above the surface while using the CLUBB scheme.

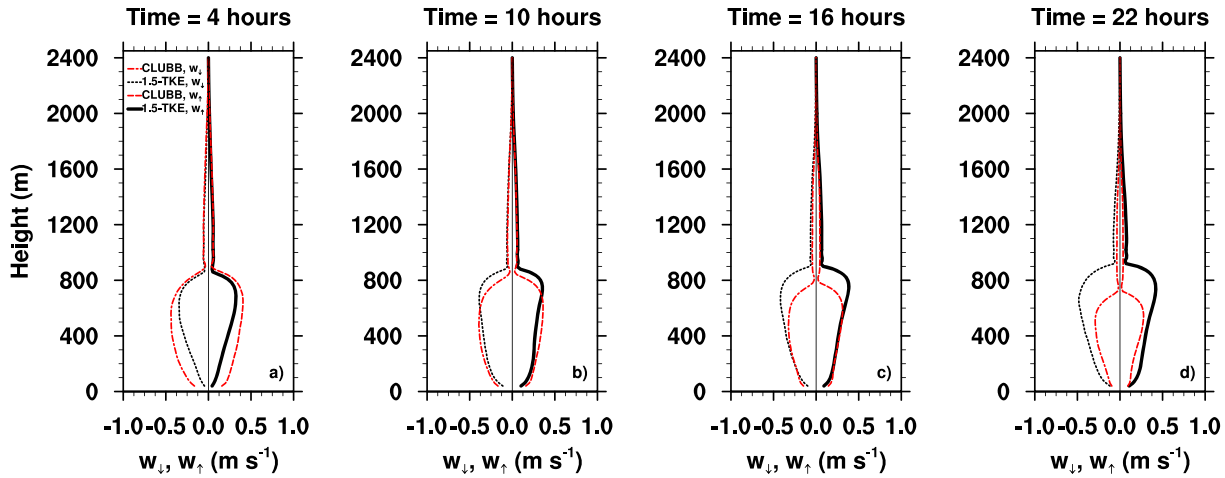

Figure 14. Profiles of the domain-averaged upward and downward vertical velocity, with the 1.5-TKE (in black) and CLUBB (in red) schemes. The profiles are at (a) 4, (b) 10, (c) 16, and (d) 22 h into the simulation.

In autumn mixed-phase clouds, *Shupe et al.* [2008] reported a circulation pattern consisting of strong, broad updrafts and weak, narrow downdrafts 5–8 km apart. The simulation produced with the 1.5-TKE scheme has periodicity of ~5 km between updrafts and downdrafts of the meso-γ-scale organization (e.g., Figures 12 and 13), and the cloud produced with the CLUBB scheme does not have this organization at all. In both simulations, however, there does not appear to be areas of narrow downdrafts as observed by *Shupe et al.* [2008]. We lack the observational data sets to claim if the organization seen in the 1.5-TKE scheme is realistic and if it represents all springtime, decoupled stratocumulus mixed-phase cloud's convective organization.

This cloud's updraft and downdraft cores might be smaller than other closed-cell stratocumulus due to the smaller precipitation rates and by corollary, strength of the downdrafts. In simulations of autumn mixed-phase clouds, precipitation rates were nearly an order of magnitude higher than the simulations here (~0.002 mm h^{-1} for 1.5-TKE mm h^{-1} and ~0.0006 for CLUBB) [*Morrison et al.*, 2008, 2011]. Additionally, precipitation rates in autumn mixed-phase stratocumulus clouds appear to be more similar to midlatitude stratocumulus than this springtime mixed-phase cloud [*Feingold et al.*, 2010; *Wood*, 2012].

The conceptual model of mixed-phase clouds in *Morrison et al.* [2012] suggests liquid forms in updrafts, ice nucleates in the cloud layer, and then ice grows rapidly which encourages sedimentation. To apply this conceptual model to our simulations, we once again assume that these simulations contain realistic aspects of

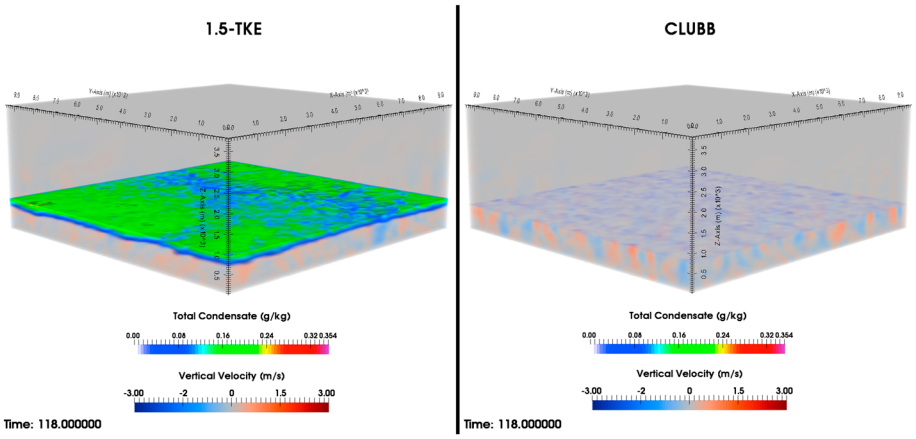

Figure 15. Total condensate (precipitating rain and snow and nonprecipitating water and ice) and the vertical velocity at 12 h into the simulation for the (left) 1.5 TKE scheme and the (right) CLUBB scheme. The total condensate is shown in the rainbow color bar, and the vertical velocity is shown with the blue-to-red color bar.

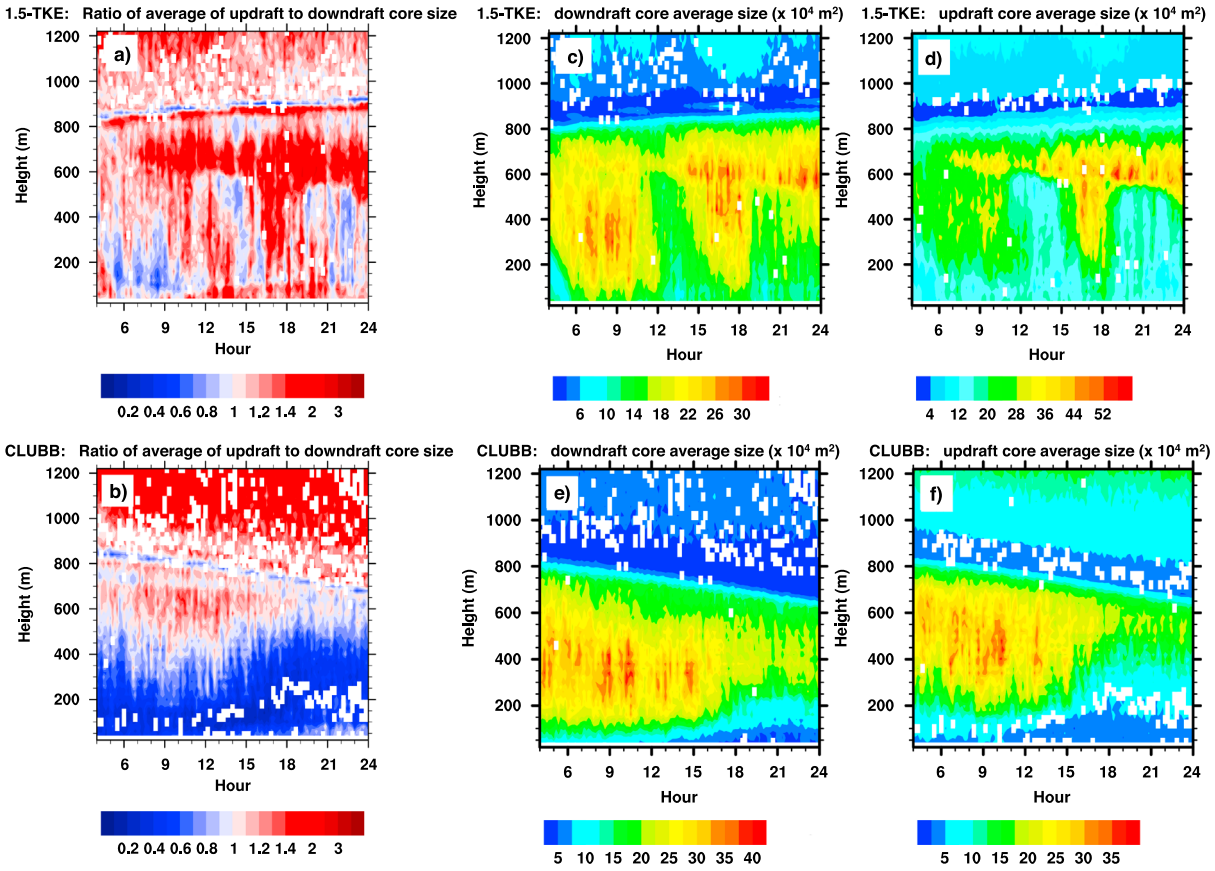

Figure 16. Ratio of the average updraft and downdraft core size for the entire domain in height as a function of time for the (a) 1.5 TKE scheme and (b) CLUBB scheme. The domain-averaged downdraft and updraft core sizes are shown for the (c and d) 1.5 TKE scheme, and the (e and f) CLUBB scheme. Please note that the values of the color bars are different in Figures 16c–16f.

the observed cloud in order to investigate the phase partitioning within the updrafts and downdrafts. Individual core sizes are measured and identified with image processing software. Slices of the LES output at every level and time step are saved as portable network graphics (PNGs), and the cores are classified as "objects" by the imaging processing software. Once identified as an object, the core size is computed from the PNG at every level and time step for both the 1.5-TKE and CLUBB schemes. Figure 16 shows the results of this computation, which is the domain-averaged mean updraft and downdraft core sizes with the CLUBB and 1.5-TKE schemes. The ratio of the average size of the cores is also presented in Figure 16. Both the 1.5-TKE and CLUBB schemes show that throughout most of the simulation in the predominantly liquid portion of the cloud, the updraft cores are bigger than the downdraft cores. This occurs between 600 m and 800 m in the cloud with the 1.5-TKE scheme and roughly between 600 m and 750 m with the CLUBB scheme. With both schemes below 600 m where the cloud is mostly ice, there are periodic times when the downdraft cores are bigger than the updraft cores. Given what is seen in Figures 12–14, one can form an appended conceptual picture of this springtime mixed-phase cloud where an "in-cloud" area might be thought of distinct from the "below-cloud" area because the average core-size ratio reverses in the column.

Figures 17 and 18 show a more detailed view of the phase of the updraft and downdraft cores 10 h into each simulation when the clouds are considered spun-up, but prior to significant liquid water depletion when the CLUBB scheme is used. An important finding is that both liquid and ice exist in both updraft and downdraft cores in both the CLUBB and 1.5-TKE simulations. Liquid exists at the top of the cloud and then is depleted at lower levels (i.e., 100 m and 300 m). The rehumidification of the near surface in the CLUBB simulation causes liquid water to be present in the updraft core at 100 m, which does not exist in the simulation when the 1.5-TKE scheme is used. Ice exists at all levels, is highest in concentration at 300 m and 600 m, and is depleted at the

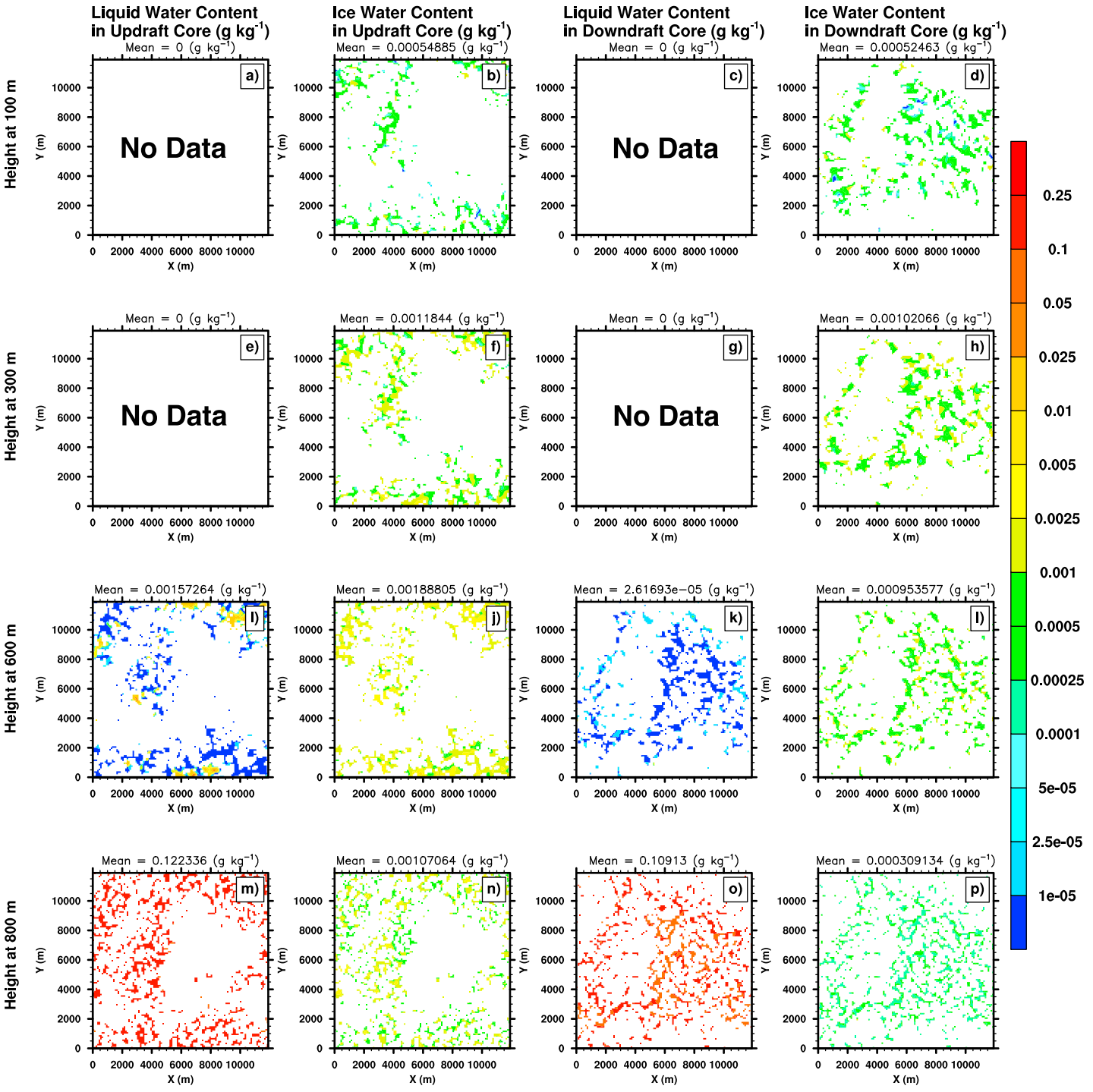

Figure 17. The liquid and ice water contents (g kg^{-1}) in the updraft and downdraft cores at (a–d) 100, (e–h) 300, (i–l) 600, and (m–p) 800 m above the surface, 10 h into the simulation for when the 1.5-TKE scheme was used. The mean value of each contour plot is given at the top of each contour plot.

surface do to warmer temperatures. Ice is the dominant phase in updaft and downdraft cores at all levels except at cloud top where liquid is dominant. Once again appending to the *Morrison et al.* [2012] conceptual model of mixed-phase clouds, we include ice to the top of the cloud base. Follow-on work would be to understand the size of the ice in relation to the phase partitioning in other mixed-phase stratocumulus clouds, such as those that are coupled to the surface.

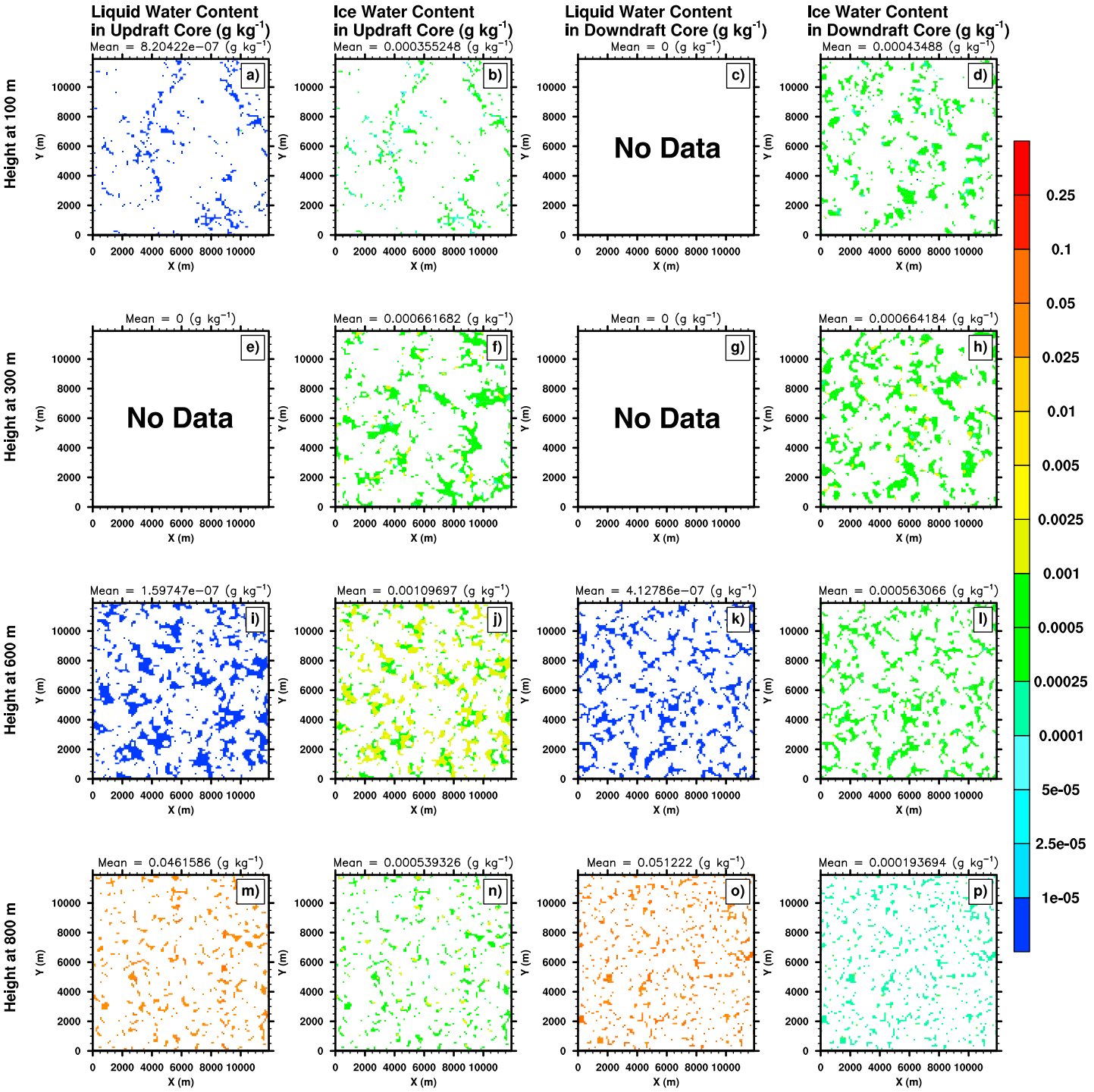

Figure 18. The liquid and ice water contents (g kg^{-1}) in the updraft and downdraft cores at (a–d) 100, (e–h) 300, (i–l) 600, and (m–p) 800 m above the surface, 10 h into the simulation for when the CLUBB scheme was used. The mean value of each contour plot is given at the top of each contour plot.

8. Summary and Conclusions

This study analyzes the macrophyscial properties of an idealized springtime Arctic mixed-phase stratocumulus cloud simulated with two different subgrid-scale turbulence schemes, 1.5-TKE and CLUBB. We showed both schemes produced a stratocumulus mixed-phase cloud with liquid at cloud top and ice precipitation toward the surface. These idealized simulations were compared with in situ aircraft measurements to provide

a basis for further analysis. This comparison revealed that the 1.5-TKE scheme produces an overly liquid cloud and the CLUBB scheme produces too little liquid water. Neither scheme was able to reproduce ice water mass or number concentration within measurement variability. Both schemes underpredicted ice water mass mixing ratio and overpredicted ice number concentration. This answered our first question in section 1, "What macroscopic differences arise in the cloud when different subgrid turbulent parameterizations are used?"

We attribute differences in liquid water path and ice water path between the two schemes to the amount of dissipative energy each subgrid scheme calculates. CLUBB is more dissipative than 1.5-TKE, causing lower in-cloud resolved and subgrid-scale turbulent kinetic energy. To increase the amount of liquid water and turbulent kinetic energy in the mixed-phase cloud with the CLUBB scheme, the turbulent length scale or the grid box size could be increased. Increasing the grid box size (i.e., Δx and Δy) showed that CLUBB appears to be more scale aware than the 1.5-TKE scheme for $\Delta x, \Delta y > 1000$ m. This is consistent with *Larson et al.* [2012], who tested CLUBB at kilometer-sized grid spacing and found improvement in simulations of cumulus and boundary layer clouds with increasing grid spacing. *Nishizawa et al.* [2015] have had similar findings in that the grid aspect ratio influences the turbulent statistics in the planetary boundary layer, and *Cheng et al.* [2010] found that increasing the resolution increases the liquid water path. As resolutions become higher in global models, there is a need for understanding parameterization performance in many environments across many scales. Exploring the impact of changing grid geometries and resolution in simulations of Arctic stratocumulus mixed-phase cloud is slated for future work.

We also asked in section 1: "What are the properties (size, strength, and phase) of the updraft and downdraft cores?" and "How do these properties compare with current knowledge of other stratocumulus cloud cores?"

We found that the 1.5-TKE scheme produces larger and stronger updraft cores and smaller, yet stronger, downdraft cores in size than the CLUBB scheme. We analyzed the phase of the cores and found that liquid water mass exists in both updraft and downdraft cores, but only in the top ~200 m of the cloud. Ice exists in both updraft and downdraft cores from the surface to the cloud top in both schemes, maximizing at the base of the liquid layer in the updraft cores. In both schemes, the updraft cores are larger in size than the downdraft cores in the liquid layer of the cloud. In the simulation with the CLUBB scheme, the downdraft cores are bigger than the updraft cores in the ice precipitation portion of the cloud. However, when the 1.5-TKE scheme is used, downdraft cores are periodically bigger than updraft cores in the ice precipitation portion of the cloud. From this relationship of core sizes throughout the column, a conceptual model is envisioned where two dominant areas of turbulent eddies exist: one in the predominantly liquid portion of the cloud and the other in the ice precipitation portion of the cloud. The cores in the 1.5-TKE scheme self-organize into a meso-γ circulation, which appears similar to the configurations of closed-cell midlatitude and Arctic autumn mixed-phase stratocumulus clouds. The cloud produced when the CLUBB scheme is used did not self-organize, and the reason behind this could lie in the differences in the overall turbulent kinetic energy in the cloud. In comparing to other stratocumulus clouds, these simulations imply that this Arctic springtime mixed-phase stratocumulus cloud's updraft and downdraft cores might generally have different sizes compared to closed-cell midlatitude and Arctic autumn mixed-phase stratocumulus clouds. In the 1.5-TKE simulation, the updrafts and downdrafts appear to be similar in size. *Shupe et al.* [2008] reported a circulation pattern consisting of strong, broad updrafts and weak, narrow downdrafts 5–8 km apart in autumn mixed-phase clouds. Midlatitude closed-cell stratocumulus are not (generally) mixed phased, and it has been found that updraft cores are large but weak, whereas the downdraft cores are small and strong [*Helfand and Kalnay*, 1983]. We attribute differences between these clouds to lower precipitation rates in this springtime mixed-phase stratocumulus cloud compared to other precipitating stratocumulus clouds.

Limitations in our findings include the idealized nature of the simulations of this one springtime Arctic mixed-phase stratocumulus cloud and assumptions within the LES configuration including the ice nucleation mechanism, aerosol size distribution and composition, and latent heat release from ice formation in CLUBB. Additional sensitivity tests could emulate perturbations of aerosols, temperature, and moisture, similar to the work of *Wang et al.* [2010] who investigated drizzle formation in open cell, closed cell, and pockets of closed cells of stratocumulus clouds in a larger domain. Follow-on work includes resolution sensitivity and convergence of cloud properties, similar to the methodology of *Cheng and Xu* [2008] and *Cheng et al.* [2010]. With more observations and modeling of springtime mixed-phase stratocumulus clouds, more knowledge can be obtained about these clouds and the relationship to their environment.

Acknowledgments
The authors would like to thank the Editor and two anonymous reviewers for their suggestions which improved our manuscript. E.L. Roesler would also like to thank Mikhail Ovchinnikov, Steven J. Ghan, Vince E. Larson, Leo Donner, and Alexei Korolev for their help and feedback regarding SAM and ISDAC. We would like to thank Marat Khairoutdinov for providing the System for Atmospheric Modeling (SAM). The Department of Energy's Global Change Education Program Graduate Research Environmental Fellowship and Sandia National Laboratories' Laboratory Directed Research and Development program funded this work. Data displayed in this paper will be curated for 5 years after publication and will be made available upon request per AGU Publications Data Policy. Sandia National Laboratories is a multimission laboratory managed and operated by Sandia Corporation, a wholly owned subsidiary of Lockheed Martin Corporation, for the U.S. Department of Energy's National Nuclear Security Administration under contract DE-AC04-94AL85000. SAND2017-3557 J.

References

Abdul-Razzak, H., and S. J. Ghan (2000), A parameterization of aerosol activation 2. Multiple aerosol types, *J. Geophys. Res.*, *105*(D5), 6837–6844.

Avramov, A., and J. Y. Harrington (2010), Influence of parameterized ice habit on simulated mixed phase Arctic clouds, *J. Geophys. Res.*, *115*, D03205, doi:10.1029/2009JD012108.

Avramov, A., et al. (2011), Toward ice formation closure in Arctic mixed-phase boundary layer clouds during ISDAC, *J. Geophys. Res.*, *116*, D00T08, doi:10.1029/2011JD015910.

Barrie, L. A. (1986), Arctic air-pollution—An overview of current knowledge, *Atmos. Environ.*, *20*(4), 643–663.

Bogenschutz, P. A., A. Gettelman, H. Morrison, V. E. Larson, C. Craig, and D. P. Schanen (2013), Higher-order turbulence closure and its impact on climate simulations in the Community Atmosphere Model, *J. Clim.*, *26*(23), 9655–9676.

Cheng, A., K.-M. Xu, and B. Stevens (2010), Effects of resolution on the simulation of boundary-layer clouds and the partition of kinetic energy to subgrid scales, *J. Adv. Model. Earth Syst.*, *2*, 3, doi:10.3894/JAMES.2010.2.3.

Cheng, A. N., and K. M. Xu (2008), Simulation of boundary-layer cumulus and stratocumulus clouds using a cloud-resolving model with low- and third-order turbulence closures, *J. Meteorol. Soc. Jpn.*, *86a*, 67–86.

Collins, W. D., P. J. Rasch, B. A. Boville, J. J. Hack, J. R. McCaa, D. L. Williamson, B. P. Briegleb, C. M. Bitz, S.-J. Lin, and M. Zhang (2006), The formulation and atmospheric simulation of the Community Atmosphere Model Version 3 (CAM3), *J. Clim.*, *19*(11), 2144–2161.

Curry, J. A., W. B. Rossow, D. Randall, and J. L. Schramm (1996), Overview of Arctic cloud and radiation characteristics, *J. Clim.*, *9*(8), 1731–1764.

de Boer, G., E. W. Eloranta, and M. D. Shupe (2009), Arctic mixed-phase stratiform cloud properties from multiple years of surface-based measurements at two high-latitude locations, *J. Atmos. Sci.*, *66*(9), 2874–2887.

Deardorff, J. W. (1980), Stratocumulus-capped mixed layers derived from a 3-dimensional model, *Boundary Layer Meteorol.*, *18*(4), 495–527.

Eicken, H. (2013), SEARCH: Study of Environmental Arctic Change. [Available at http://www.arcus.org/search/.]

European Centre for Medium-Range Weather Forecasts (2009), *ERA-Interim*, Project Res. Data Archive at the Natl. Cent. for Atmos. Res., Comput. and Inf. Syst. Lab.

Fan, J. W., M. Ovtchinnikov, J. M. Comstock, S. A. McFarlane, and A. Khain (2009), Ice formation in Arctic mixed-phase clouds: Insights from a 3-D cloud-resolving model with size-resolved aerosol and cloud microphysics, *J. Geophys. Res.*, *114*, D04205, doi:10.1029/2008JD010782.

Feingold, G., I. Koren, H. L. Wang, H. W. Xue, and W. A. Brewer (2010), Precipitation-generated oscillations in open cellular cloud fields, *Nature*, *466*(7308), 849–852.

Field, P. R., A. J. Heymsfield, and A. Bansemer (2006), Shattering and particle interarrival times measured by optical array probes in ice clouds, *J. Atmos. Oceanic Technol.*, *23*(10), 1357–1371.

Francis, J. A., and S. J. Vavrus (2012), Evidence linking Arctic amplification to extreme weather in mid-latitudes, *Geophys. Res. Lett.*, *39*, L06801, doi:10.1029/2012GL051000.

Ghan, S. J., et al. (2007), *Science Overview Document Indirect and Semi-Direct Aerosol Campaign (ISDAC) April 2008*.

Golaz, J. C., V. E. Larson, and W. R. Cotton (2002), A PDF-based model for boundary layer clouds. Part I: Method and model description, *J. Atmos. Sci.*, *59*(24), 3540–3551.

Helfand, H. M., and E. Kalnay (1983), A model to determine open or closed cellular convection, *J. Atmos. Sci.*, *40*(3), 631–650.

Intrieri, J. M., C. W. Fairall, M. D. Shupe, P. O. G. Persson, E. L. Andreas, P. S. Guest, and R. E. Moritz (2002), An annual cycle of Arctic surface cloud forcing at SHEBA, *J. Geophys. Res.*, *107*(C10), 8039, doi:10.1029/2000JC000439.

Khairoutdinov, M. F., and D. A. Randall (2003), Cloud resolving modeling of the ARM summer 1997 IOP: Model formulation, results, uncertainties, and sensitivities, *J. Atmos. Sci.*, *60*(4), 607–625.

Klein, S. A., et al. (2009), Intercomparison of model simulations of mixed-phase clouds observed during the ARM Mixed-Phase Arctic Cloud Experiment I: Single-layer cloud, *Q. J. R. Meteorol. Soc.*, *135*(641), 979–1002.

Krishnamurti, R. (1975), On cellular cloud patterns. Part 1: Mathematical model, *J. Atmos. Sci.*, *32*(7), 1353–1363.

Larson, V. E., J.-C. Golaz, and W. R. Cotton (2002), Small-scale and mesoscale variability in cloudy boundary layers: Joint probability density functions, *J. Atmos. Sci.*, *59*(24), 3519–3539.

Larson, V. E., D. P. Schanen, M. H. Wang, M. Ovchinnikov, and S. Ghan (2012), PDF parameterization of boundary layer clouds in models with horizontal grid spacings from 2 to 16 km, *Mon. Weather Rev.*, *140*(1), 285–306.

McFarquhar, G. M., G. Zhang, M. R. Poellot, G. L. Kok, R. McCoy, T. Tooman, A. Fridlind, and A. J. Heymsfield (2007), Ice properties of single-layer stratocumulus during the Mixed-Phase Arctic Cloud Experiment: 1. Observations, *J. Geophys. Res.*, *112*, D24201, doi:10.1029/2007JD008633.

McFarquhar, G. M., et al. (2011), Indirect and Semi-Direct Aerosol Campaign: The impact of Arctic aerosols on clouds, *Bull. Am. Meteorol. Soc.*, *92*(2), 183–201.

Morrison, H., J. A. Curry, and V. I. Khvorostyanov (2005), A new double-moment microphysics parameterization for application in cloud and climate models. Part I: Description, *J. Atmos. Sci.*, *62*(6), 1665–1677.

Morrison, H., J. O. Pinto, J. A. Curry, and G. M. McFarquhar (2008), Sensitivity of modeled Arctic mixed-phase stratocumulus to cloud condensation and ice nuclei over regionally varying surface conditions, *J. Geophys. Res.*, *113*, D05203, doi:10.1029/2007JD008729.

Morrison, H., et al. (2011), Intercomparison of cloud model simulations of Arctic mixed-phase boundary layer clouds observed during SHEBA/FIRE-ACE, *J. Adv. Model. Earth Syst.*, *3*, M05001, doi:10.1029/2011MS000066.

Morrison, H., G. de Boer, G. Feingold, J. Harrington, M. D. Shupe, and K. Sulia (2012), Resilience of persistent Arctic mixed-phase clouds, *Nat. Geosci.*, *5*(1), 11–17.

Nishizawa, S., H. Yashiro, Y. Sato, Y. Miyamoto, and H. Tomita (2015), Influence of grid aspect ratio on planetary boundary layer turbulence in large-eddy simulations, *Geosci. Model Dev.*, *8*(10), 3393–3419, doi:10.5194/gmd-8-3393-2015.

Orlanski, I. (1975), Rational subdivision of scales for atmospheric processes, *Bull. Am. Meteorol. Soc.*, *56*(5), 527–530.

Ovchinnikov, M., A. Korolev, and J. W. Fan (2011), Effects of ice number concentration on dynamics of a shallow mixed-phase stratiform cloud, *J. Geophys. Res.*, *116*, D00T06, doi:10.1029/2011JD015888.

Ovchinnikov, M., et al. (2014), Intercomparison of large-eddy simulations of Arctic mixed-phase clouds: Importance of ice size distribution assumptions, *J. Adv. Model. Earth Syst.*, *6*, 223–248, doi:10.1002/2013MS000282.

Qiu, S. Y., X. Q. Dong, B. Xi, and J. L. F. Li (2015), Characterizing Arctic mixed-phase cloud structure and its relationship with humidity and temperature inversion using ARM NSA observations, *J. Geophys. Res. Atmos.*, *120*, 7737–7746, doi:10.1002/2014JD023022.

Roesler, E. L., and J. E. Penner (2010), Can global models ignore the chemical composition of aerosols?, *Geophys. Res. Lett.*, *37*, L24809, doi:10.1029/2010GL044282.

Shupe, M. D., T. Uttal, and S. Y. Matrosov (2005a), Arctic cloud microphysics retrievals from surface-based remote sensors at SHEBA, *J. Appl. Meteorol.*, *44*(10), 1544–1562.

Shupe, M. D., T. Uttal, and S. Y. Matrosov (2005b), Arctic cloud microphysics retrievals from surface-based remote sensors at SHEBA, *J. Appl. Meteorol.*, *44*(10), 1544–1562.
Shupe, M. D., S. Y. Matrosov, and T. Uttal (2006), Arctic mixed-phase cloud properties derived from surface-based sensors at SHEBA, *J. Atmos. Sci.*, *63*(2), 697–711.
Shupe, M. D., P. Kollias, P. O. G. Persson, and G. M. McFarquhar (2008), Vertical motions in Arctic mixed-phase stratiform clouds, *J. Atmos. Sci.*, *65*(4), 1304–1322.
Shupe, M. D., P. O. G. Persson, I. M. Brooks, M. Tjernström, J. Sedlar, T. Mauritsen, S. Sjogren, and C. Leck (2013), Cloud and boundary layer interactions over the Arctic sea ice in late summer, *Atmos. Chem. Phys.*, *13*(18), 9379–9399.
Solomon, A., M. D. Shupe, P. O. G. Persson, and H. Morrison (2011), Moisture and dynamical interactions maintaining decoupled Arctic mixed-phase stratocumulus in the presence of a humidity inversion, *Atmos. Chem. Phys.*, *11*(19), 10,127–10,148.
Storer, R. L., B. M. Griffin, J. Höft, J. K. Weber, E. Raut, V. E. Larson, M. Wang, and P. J. Rasch (2015), Parameterizing deep convection using the assumed probability density function method, *Geosci. Model Dev.*, *8*(1), 1–19, doi:10.5194/gmd-8-1-2015.
Stroeve, J. C., V. Kattsov, A. Barrett, M. Serreze, T. Pavlova, M. Holland, and W. N. Meier (2012), Trends in Arctic sea ice extent from CMIP5, CMIP3 and observations, *Geophys. Res. Lett.*, *39*, L16502, doi:10.1029/2012GL052676.
Sulia, K. J., H. Morrison, and J. Y. Harrington (2014), Dynamical and microphysical evolution during mixed-phase cloud glaciation simulated using the bulk adaptive habit prediction model, *J. Atmos. Sci.*, *71*(11), 4158–4180.
Turner, D. D., et al. (2007), Thin liquid water clouds: Their importance and our challenge, *Bull. Am. Meteorol. Soc.*, *88*(2), 177–190.
Wang, H., G. Feingold, R. Wood, and J. Kazil (2010), Modelling microphysical and meteorological controls on precipitation and cloud cellular structures in southeast Pacific stratocumulus, *Atmos. Chem. Phys.*, *10*(13), 6347–6362, doi:10.5194/acp-10-6347-2010.
Wood, R. (2012), Stratocumulus clouds, *Mon. Weather Rev.*, *140*(8), 2373–2423, doi:10.1175/MWR-D-11-00121.1.
Xie, S. C., S. A. Klein, M. H. Zhang, J. J. Yio, R. T. Cederwall, and R. McCoy (2006), Developing large-scale forcing data for single-column and cloud-resolving models from the Mixed-Phase Arctic Cloud Experiment, *J. Geophys. Res.*, *111*, D19104, doi:10.1029/2005JD006950.
Zelenyuk, A., D. Imre, M. Earle, R. Easter, A. Korolev, R. Leaitch, P. Liu, A. M. Macdonald, M. Ovchinnikov, and W. Strapp (2010), In situ characterization of cloud condensation nuclei, interstitial, and background particles using the single particle mass spectrometer, SPLAT II, *Anal. Chem.*, *82*(19), 7943–7951.
Zhang, M. H., and J. L. Lin (1997), Constrained variational analysis of sounding data based on column-integrated budgets of mass, heat, moisture, and momentum: Approach and application to ARM measurements, *J. Atmos. Sci.*, *54*(11), 1503–1524.
Zhang, M. H., J. L. Lin, R. T. Cederwall, J. J. Yio, and S. C. Xie (2001), Objective analysis of ARM IOP data: Method and sensitivity, *Mon. Weather Rev.*, *129*(2), 295–311.